Title
Distinct signaling requirements underlie beige fat recruitment in development versus adulthood

Author
Wu, Yixuan

Publication Date
2019

Peer reviewed|Thesis/dissertation

Distinct signaling requirements underlie beige fat recruitment in development versus adulthood.

by
Yixuan Wu

DISSERTATION
Submitted in partial satisfaction of the requirements for degree of
DOCTOR OF PHILOSOPHY

in

Biomedical Sciences

in the

GRADUATE DIVISION
of the
UNIVERSITY OF CALIFORNIA, SAN FRANCISCO

Approved:

DocuSigned by:
Clifford Lowell
1EA1A95C4F734C7...

Clifford Lowell
Chair

DocuSigned by:
Ajay Chawla
[illegible]

Ajay Chawla

DocuSigned by:
Christopher D. C. Allen
[illegible]

Christopher D. C. Allen

DocuSigned by:
A. Brack
8019548714A4420...

Andrew Brack

Committee Members

Dedicated foremost to my family, as well as

all the teachers who believed in me over the years

ACKNOWLEDGEMENTS

I would like to begin by thanking Ajay Chawla for his mentorship throughout this incredible journey. Graduate school is in many respects like a traditional apprenticeship; a novice goes through hands-on vocational training under a master's tutelage, after which he becomes a journeyman in his own right. I have learned much from Ajay over the years which I hope to incorporate into my own approach to science and life in general. He is a finder of paths unseen and is insatiably curious about all facets of science, qualities which have manifested themselves in the myriad research projects within the lab. By asking questions that lie at the intersection of different biological fields, the lab has been able to instigate new avenues of research while simultaneously improving our understanding of the pre-existing terrain. This thesis perhaps inadvertently encapsulates this spirit by incorporating aspects of metabolism, developmental biology, neuroscience, immunology, and genetics/epigenetics. Ajay is also unapologetically devoted to his family; both he and his wife have managed to pursue highly-demanding careers while raising three children. As the icing on the cake, they have no social media presence(!), which is a laudable achievement in this age of persistent push notifications and pernicious pseudonymous personas. Like SF, my years in graduate school were often beset by fog, and I am grateful to Ajay for bringing clarity in such times. By giving me the freedom to experiment and fail, he gave me the space to develop into the scientist I am today.

I would also like to thank my committee members Cliff Lowell, Andrew Brack, and Chris Allen. I'm sure they suffered from severe whiplash with all the project changes over the years, but the final product is far better for their feedback and critique. I am grateful that they stuck it out despite the topic being very different from their personal areas of interest (especially Andrew!) and took the time to guide me in terms of both the science and being a scientist.

As you all know, the lab is the actual room where it happens. I am grateful to the members of the Chawla lab (past and present) for creating a fun workspace and for just being

stand-up folks. Each research lab is a distinct unit unto itself, and one quickly learns that trust and openness are critical for the entire operation to work. Many thanks to my fellow ~~minions~~ grad students Nyasha Chagwedera and Vassily Kutyavin; we all joined the lab at around the same time and having peers to lean on was essential to my well-being. Thank you to our lab manager Xiaojin Cui who kept everything oiled and running (against all odds), and especially for running all our mouse genotyping reactions for us (my PhD would have taken twice as long without this part). Thank you to Melissa Kinnebrew for being a fantastic collaborator (together with Vassily), as well as for being a friend and mentor (especially during this final stretch). Thank you to Kirthana Ganeshan for being the scientific and spiritual core of the lab, as well as the other (honorary) Southeast Asian representative in the area. Finally, a special shout-out to Justin Odegaard and Lata Mukundan who got me settled and taught me everything I needed to learn when I first joined the lab.

Thank you to the administrators at the UCSF Biomedical Sciences graduate program, especially Demian Sainz, Lisa Magargal, Ned Molyneaux, and Monique Piazza. Navigating grad school (especially as an international student) was infinitely less stressful knowing that they had my back. Many thanks as well to DeLaine Larsen and Kari Herrington at the Nikon Imaging Center for teaching me how to use the light sheet microscope, without which my project would never have gotten off the ground.

Thank you to the BMS class of 2013 for being wonderful companions on this years-long journey. Special shout-out to the pub trivia / board games / Game of Thrones crew. We had a good run terrorizing unsuspecting casuals on a weekly basis, and they will whisper our (many, many) team names for years to come. I'm also incredibly grateful to my fellow Singaporeans who helped create (quite literally) a home away from home. There's nothing quite like being able to lapse into Singlish at the end of an exhausting day. Thanks for the culinary escapades and epic Spirit Island games, and I hope there will be more to come in the future.

There is a Chinese idiom, 饮水思源, which translates literally to "when you drink water, remember the source". I am especially grateful to my family who built the foundation and then allowed me to grow into the person I am today. Thank you for your unwavering support throughout all these years of living abroad, for keeping a politely straight face when I attempt to explain things that made more sense in my head at the time, and for keeping me rooted back home in spirit if not in person.

Last but certainly not least, thank you Meera, the best of wives and best of women. You are the moon of my life, the light at the end of the tunnel, my never-ending source of joy and inspiration. As a wise man once said, "if it takes fighting a war for us to meet, it will have been worth it". Grad school has been a challenging experience, but it was made all the richer for your presence by my side. You are my best friend, counsellor, and partner-in-crime, and I look forward to all the adventures we'll have together (P.S: I still get to be party leader though).

Contributions to the Presented Work

Chapter 2:

Chapter 2 of this dissertation contains work that is being prepared for submission as a manuscript. I performed all microscopy and sequencing library preparation under the guidance of Ajay Chawla. Sequencing data was analyzed together with Vassily Kutyavin. Immunoblotting was performed by Vassily Kutyavin. Ajay Chawla supervised the entirety of this work.

Chapter 3:

Chapter 3 of this dissertation contains work that is being prepared for submission as a manuscript. I performed all microscopy assays under the guidance of Ajay Chawla. Oxygen consumption and cold tolerance assays were performed in conjunction with Melissa Kinnebrew. Sequencing library preparation was performed in conjunction with Melissa Kinnebrew, and sequencing data was analyzed together with Vassily Kutyavin. Immunoblotting was performed by Vassily Kutyavin. Ajay Chawla supervised the entirety of this work.

Distinct signaling requirements underlie beige fat recruitment in development versus adulthood

Yixuan Wu

Abstract

In adult mammals, beige fat is recruited in response to environmental cold in order to generate heat (thermogenesis) and maintain a constant body temperature. It is also transiently and physiologically induced in postnatal animals; however, little is known about how this process is regulated. Here, we use light sheet microscopy, high throughput sequencing, and metabolic assays to show that although the spatiotemporal kinetics of recruitment are very similar in young and adult mice, distinct regulatory signals prevail at each time point. Systemic adrenergic signaling or environmental cold stimulus is required only for beiging in adult, but not postnatal animals. In contrast, postnatal beiging depends on tissue- and cell-intrinsic pathways such as type 2 cytokines and adipocyte B-cell lymphoma 6 (BCL6) respectively. In adults, BCL6 is required for neither transdifferentiation of naïve adipocytes, nor reactivation of dormant cells. Together, our findings reveal an unexpected distinction between beige fat regulation in postnatal and adult animals, thereby introducing a previously-unappreciated temporal dimension to the study of the beiging process.

Table of Contents

Chapter 1 : Introduction 1

Chapter 2 : Postnatal and adult beige fat are recruited in a similar spatiotemporal pattern, but are differentially dependent on adrenergic signaling. 7

ABSTRACT 8

INTRODUCTION 9

RESULTS 10

DISCUSSION 16

METHODS 23

Chapter 3 : BCL6 and type 2 cytokines play complex roles in beiging 29

ABSTRACT 30

INTRODUCTION 31

RESULTS 32

DISCUSSION 38

METHODS 43

Chapter 4 : Concluding Remarks and Future Directions 48

References 52

List of Figures

Chapter 1

Figure 1.1: Sources of beige adipocytes in postnatal and adult iWAT 6

Chapter 2

Figure 2.1: Beiging follows a fixed spatiotemporal pattern in both young and adult iWAT. 18

Figure 2.2: Young and adult beige fat are transcriptionally and epigenetically distinct.....19

Figure 2.3: SNS innervation of iWAT is dispensable for postnatal beiging. 20

Figure 2.4: Postnatal iWAT develops differently under thermoneutral versus SNS-deficient conditions. 21

Figure 2.5: Adrenergic signaling is absolutely required for adult cold-induced recruitment. 22

Chapter 3

Figure 3.1: Adipocyte BCL6 is required for postnatal beiging but regulates distinct transcriptional pathways from cold-induced beige. 40

Figure 3.2: BCL6 is required for cold-induced beiging in adults, but not reactivation of dormant adipocytes.....41

Figure 3.3: Immune signals play complicated roles in postnatal and adult beiging. 42

Chapter 1 :

Introduction

The plan is, to fan this spark into a flame.

—Lin-Manuel Miranda, *Hamilton: An American Musical*

Adaptive thermogenesis: nature's thermostat

Maintenance of a steady internal body temperature is critical for the survival of almost all organisms, as this is necessary for the proper functioning of the myriad biochemical processes that sustain life (Cannon and Nedergaard 2004; M. Harms and Seale 2013). Homeothermic organisms have therefore evolved various mechanisms to defend their optimal body temperature from fluctuations in environmental conditions. These thermoregulatory strategies fall into two broad categories: ectothermy, which relies on behavioral adaptations (e.g. basking in the sun), and endothermy, which utilizes internal metabolic processes (e.g. shivering). One major endothermic mechanism is 'adaptive thermogenesis'; which, like a thermostat, can be modulated in proportion to the organism's homeostatic demands.

Adaptive thermogenesis occurs in both brown and beige adipocytes, which are found in brown adipose tissue (BAT) and white adipose tissue (WAT) respectively (M. Harms and Seale 2013; Y. Lee et al. 2019; Wu et al. 2012). While BAT is a dedicated thermogenic organ, beige adipocytes are only recruited when necessary to respond to cold stimulus and revert to energy-storing white adipocytes when the stimulus is removed. At the systemic level, this cold-response circuit consists of afferent temperature-sensing neurons, the hypothalamus, and efferent neurons of the sympathetic nervous system (SNS), which directly innervate adipocytes in both BAT and WAT (Slavin and Ballard 1978; W. Zeng et al. 2015; Zhang and Bi 2015). At the molecular level, brown and beige adipocytes share various molecular markers, in particular uncoupling protein 1 (UCP1) which short-circuits the mitochondrial electron transport chain (ETC), diverting its energy towards heat production instead of adenosine tris-phosphate (ATP) synthesis. This locally-generated heat is then distributed throughout the organism via the circulatory system.

Beige fat recruitment: an age-old question, and a question of age

There has been considerable interest in understanding how beige fat is regulated due to its therapeutic potential for combating metabolic diseases such as obesity and diabetes, which ultimately stem from excessive energy intake (Nedergaard and Cannon 2014; M. Harms and Seale 2013). In adult mice, beige adipocytes are derived from two distinct sources: *de novo* differentiation from adipogenic precursors, and transdifferentiation from mature white adipocytes (Contreras et al. 2014; Berry and Rodeheffer 2013; Y. Lee, Petkova, and Granneman 2013; Q. A. Wang et al. 2013), though their relative contribution is the subject of much debate (Gulyaeva, Dempersmier, and Sul 2019). In either case, upon rewarming after cold exposure, beige adipocytes become dormant white adipocytes (Rosenwald et al. 2013), underscoring the reversibility of the beiging process (Fig. 1.1).

In addition to the cold-sensing circuit which involves systemic coordination between multiple organs, various local signals have been identified at both the tissue and cellular levels. For instance, inguinal WAT (iWAT)-resident type 2 myeloid cells secrete cytokines which drive differentiation of precursors into beige adipocytes, while the drug rosiglitazone can induce UCP1 expression by activating nuclear receptor peroxisome proliferator-activated γ (PPARγ) (Nedergaard and Cannon 2014; Odegaard et al. 2016; M.-W. Lee et al. 2014; Qiu et al. 2014). The vast majority of these studies have been conducted in cold-challenged adult animals; however, beige fat (as defined by UCP1 expression in iWAT) is also present postnatally from as early as p14 and decaying by around p42. Besides these UCP1 expression kinetics, little else is known about how the process is regulated at this early time point (Master et al. 2002; Gouon-Evans and Pollard 2002; Chabowska-Kita et al. 2015).

Postnatal beige fat: a fateful blindspot

Although iWAT plays similar lipid storage roles at both postnatal and adult time points (Hong et al. 2015), there are several fundamental differences between the two settings. For instance under baseline conditions, postnatal iWAT contains adipogenic precursors undergoing various stages of differentiation, whereas adult iWAT contains either uncommitted precursors or mature adipocytes (Q. A. Wang et al. 2013). This is because iWAT adipocyte differentiation (as indicated by adiponectin expression) begins in embryonic development in the third week of gestation and continues into the postnatal period (Q. A. Wang et al. 2013), i.e. the pool of available 'recruits' is different at each time point.

Another major difference is dependence on environmental temperature; one study reported that postnatal beige fat was induced even in mice housed at 30°C (i.e. thermoneutrality), albeit at weaker levels than in mice housed at 17°C (Chabowska-Kita et al. 2015). Furthermore, they found that postnatal housing temperature had no effect on the robustness of the adult cold-response. These results implied that the postnatal beiging process is to some extent temperature-insensitive and therefore driven by some internal impetus, in stark contrast to adult beiging which is strictly induced by environmental cold or adrenergic stress (Cannon and Nedergaard 2004). Identifying the intrinsic signals that drive postnatal beiging will be essential to improving our understanding of this phenomenon.

This is biologically relevant because postnatal beige adipocytes persist into adulthood and contribute significantly to the cold response at that later stage (Y. Wang et al. 2017). In other words, modulating beige fat recruitment during the postnatal period may have long-term consequences for the organism's ability to mount a cold response in the future. Indeed, there is a precedent for developmental signals playing a 'licensing' role, whereby interleukin-33 (IL-33) signaling is required during postnatal development for proper splicing of Ucp1 mRNA; in its

absence, brown and beige adipocytes develop normally but are thermogenically non-functional (Odegaard et al. 2016).

The existence of postnatal beige fat also has several broader implications. Firstly, it skews the premise of the *de novo* differentiation versus transdifferentiation debate, because the latter actually comprises both first-time activation of naïve adipocytes and reactivation of dormant adipocytes that had expressed UCP1 postnatally (Fig. 1.1). Secondly, it complicates the use of constitutive knockout (KO) mouse models, because any phenotype observed in cold-challenged adults could be partially or even entirely due to perturbation at the postnatal time point. Thirdly, it challenges the interpretation of multiple studies that utilized lineage-tracing mouse models to map beige adipogenesis, especially if they had assumed that iWAT adipocytes from mice housed at room temperature (RT) or thermoneutrality (30^{o}C) had never expressed UCP1 or other thermogenic genes before (Rosenwald et al. 2013; Q. A. Wang et al. 2018; Roh et al. 2018).

This dissertation is a deep-dive into how postnatal beige fat compares to its adult counterpart / future self at the spatial, regulatory, and transcriptional levels. We report that although beige fat is spatially and functionally similar at both time points, the two are dependent on distinct signaling pathways, thereby introducing a previously-unappreciated temporal dimension to the study of beige fat.

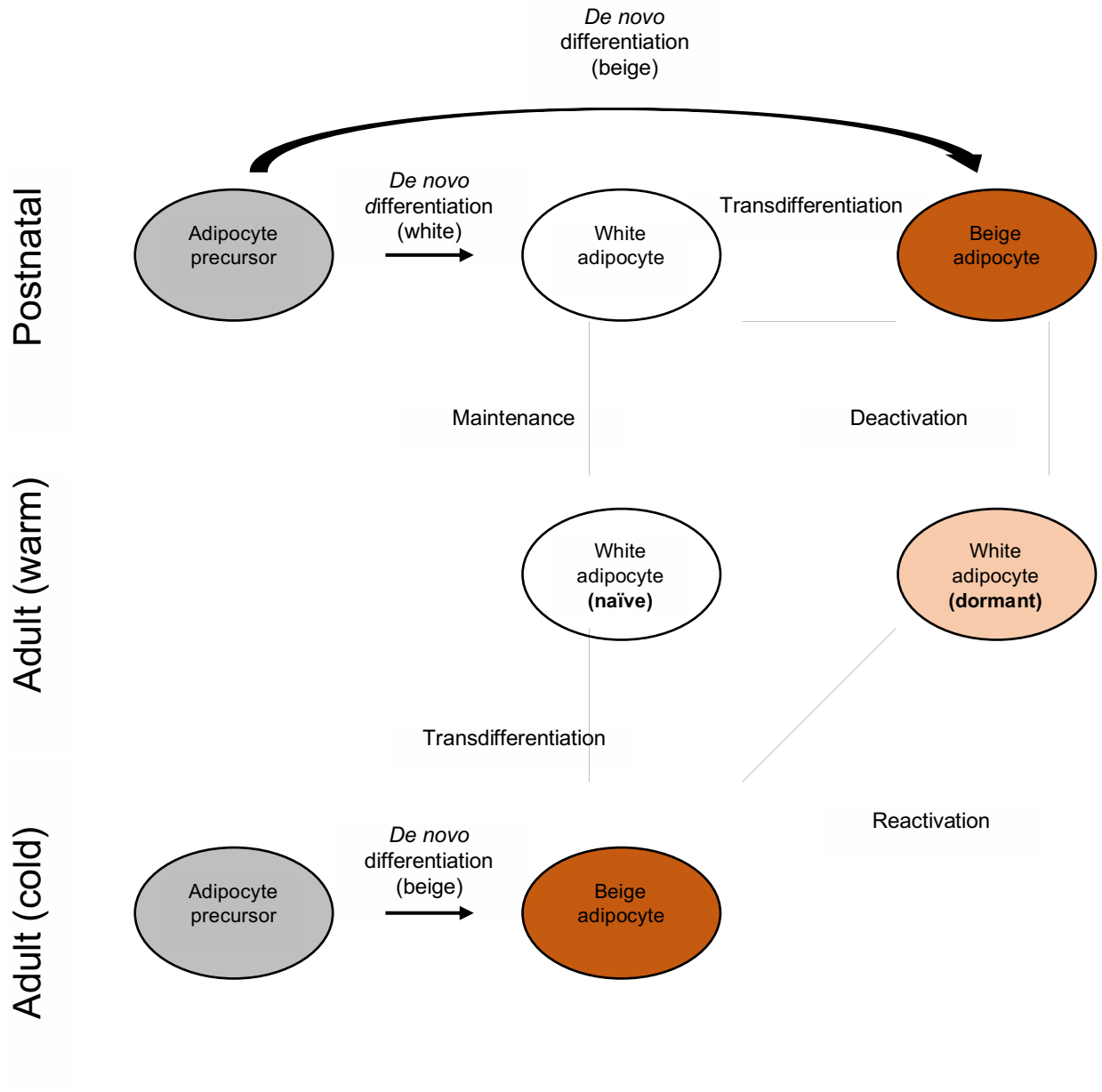

Figure 1.1: Sources of beige adipocytes in postnatal and adult iWAT

A subset of adipocytes in postnatal iWAT are beige and may be derived either directly from precursor differentiation or via a mature white adipocyte intermediate. These beige adipocytes become inactive white adipocytes as the animal matures. Upon cold stimulation of the adult, new beige adipocytes may be recruited via *de novo* differentiation, transdifferentiation of white adipocytes that did not undergo prior beiging, or reactivation of ex-beige adipocytes.

Chapter 2 :

Postnatal and adult beige fat are recruited in a similar spatiotemporal pattern, but are differentially dependent on adrenergic signaling.

If we lay a strong enough foundation, we'll pass it onto you.

We'll give the world to you, and you'll blow us all away.

—Lin-Manuel Miranda, *Hamilton: An American Musical*

ABSTRACT

In mice, beige fat is recruited either in response to environmental cold, or physiologically during postnatal development. However, little is known about how the latter process occurs, and whether it depends on the same cues as the former. Here we used light sheet microscopy to show that although the beige marker uncoupling protein 1 (UCP1) is expressed in a consistent spatiotemporal pattern in both postnatal and adult inguinal white adipose tissue (iWAT), only adult beiging requires environmental cold or sympathetic nervous system (SNS) innervation. Furthermore, RNA and ChIP sequencing revealed that postnatal and adult beige fat have distinct transcriptional and epigenetic profiles. Together, our findings reveal an unexpected distinction between regulation of beige fat in postnatal versus adult animals.

INTRODUCTION

Maintenance of a constant internal body temperature in the face of environmental fluctuations is crucial for the operation of basic physiological processes (Cannon and Nedergaard 2011). In mammals and other endotherms, two key mechanisms for heat generation are shivering and adaptive thermogenesis, the latter of which is driven primarily by brown adipose tissue (BAT) function (Cannon and Nedergaard 2004). An organism's thermogenic capacity is also enhanced by the recruitment of beige adipocytes, which are brown-like adipocytes found in white adipose tissue (WAT). Unlike BAT which remains poised for activation when not in use (e.g. under warm conditions), beige fat is induced by cold stimuli in a reversible manner, reverting to energy-storage duty when no longer required (Nedergaard and Cannon 2014). Said stimuli are recognized by the hypothalamus, which then transmits activation signals to BAT and WAT via the sympathetic nervous system (SNS) (Chi et al. 2018; W. Zeng et al. 2015; X. Zeng et al. 2019).

In adult mice, these adrenergic signals induce beiging primarily via two distinct mechanisms: *de novo* differentiation from precursors and transdifferentiation from mature white adipocytes (Y.-H. Lee et al. 2012; Rosenwald et al. 2013). Beiging also occurs in postnatal animals, including under thermoneutral housing conditions (Chabowska-Kita et al. 2015; Odegaard et al. 2016), though little is understood about how postnatal beige compares to adult at the molecular and regulatory levels. Besides their transient thermogenic activity during this period, postnatal beige adipocytes also persist into adulthood in a dormant (UCP1-negative) state (Chabowska-Kita and Kozak 2016) and can be reactivated in response to adrenergic signals (Y. Wang et al. 2017), thereby playing a recurring role in thermogenesis throughout the organism's lifetime. However, the overwhelming majority of studies in the field are performed on adult animals while completely ignoring the postnatal time point, even though the developmental

history of the tissue (and indeed the organism itself) may have far-reaching consequences in adult life (Stearns 1992).

Here we compared beiging in postnatal and adult animals and found that although the distribution of beige adipocytes and SNS nerves was remarkably similar at both time points, cold stimulus / adrenergic signaling were only required for beiging in adults. These findings raise important questions such as what other signals might be required for postnatal beiging, and whether those signals play distinct roles at each time point.

RESULTS

Beiging follows a fixed spatiotemporal pattern in both young and adult iWAT.

To establish the spatiotemporal characteristics of beiging at the postnatal time point, we performed UCP1 staining in cleared whole inguinal WAT (iWAT) from BL/6J mice at various ages. We observed expression of UCP1 protein as early as p7, which increased progressively from p14 to p28, and started to decrease by p35 (Fig. 2.1A). Upon analyzing tissues from multiple independent litters, several recurrent patterns began to emerge. Firstly, UCP1 was always expressed earlier in the inguinal (ING) arm of the iWAT (as demarcated by the lymph node) than the dorsolumbar (DL). Secondly, expression in DL always decayed more rapidly than in ING. Together, these observations suggest that the ING half is predisposed towards beiging, perhaps due to either a spatial bias of the initiating signal(s), or intrinsic differences in the mature adipocytes and precursors populations. In addition, UCP1 expression did not clearly radiate from any one point of origin, and discrete $UCP1^{+}$ adipocytes were visible, especially in the DL arm.

Adrenergic tone (e.g. in response to environmental cold stress) is a key driver of beiging in adult iWAT (Cannon and Nedergaard 2011); we therefore asked whether such external

conditions were necessary for postnatal beige development. As room temperature (RT) already represents a mild thermal stress to mice, we analyzed iWAT from BL/6J mice that were born and raised under thermoneutral conditions (30^{o}C) (Fig. 2.1B). We observed that UCP1 expression was still present at reduced levels from p21-p35 as compared to RT (Fig. 2.1C), implying that postnatal beiging is only partially dependent on environmental cold.

Next, we investigated the spatiotemporal distribution of adult cold-induced beiging by imaging iWAT from adult mice that had been housed at 8^{o}C for 2-6 days. We observed minimal baseline UCP1 expression in RT controls, while iWAT from cold-exposed mice showed a strikingly similar expression pattern to postnatal iWAT (Fig. 2.1D). This raised the intriguing possibility that some of these UCP1^{+} beige adipocytes in adult iWAT may have been the same cells that had expressed UCP1 postnatally. Indeed, postnatal depletion of UCP1^{+} cells with diphtheria toxin impairs cold-induced beiging in later life, which implies that reactivation of dormant ex-UCP1^{+} adipocytes is a major source of beiging in adults (Y. Wang et al. 2017). To verify the longevity of the postnatal UCP1^{+} adipocytes, we used a lineage tracing mouse model (CAG-LSL-tomato Ucp1^{Cre}) in which all cells with a history of UCP1 expression were permanently labeled with TdTomato. Imaging of iWAT from 20-wk-old reporter mice housed at RT showed that a considerable proportion of adipocytes were TdTomato-positive, even though the mice had never been exposed to cold (sub-RT) temperatures before (Fig. 2.1E). Furthermore, the distribution of ex-UCP1 adipocytes was identical to what had been previously observed in postnatal and adult cold-activated iWAT, strongly implying that postnatal beige adipocytes enter a dormant UCP1^{-} state as the animal matures and can be reactivated by cold exposure in adult life.

Finally, as an orthogonal approach to the imaging data, we performed a Western blot for UCP1 protein in iWAT from BL/6J mice housed at RT and observed a similar temporal pattern of weak expression at 1 week, which increased at 4 weeks, before decaying with maturity (Fig.

2.1F). Hematoxylin and eosin (H&E) staining of iWAT sections from p28 animals showed increased histological beiging in samples from mice housed at RT compared to 30C (Fig. 2.1G), providing additional evidence that postnatal beiging was indeed occurring (as opposed to merely expression of UCP1 protein).

p28 and adult beige fat are transcriptionally and epigenetically distinct.

We next wanted to compare the transcriptional profiles of postnatal and adult beige adipocytes. To address this question, we performed RNA sequencing of iWAT from p28 BL/6J mice that were born and housed at either RT or 30^{o}C, as well as iWAT from 9-wk-old BL/6J mice that had been either housed at RT or at 4^{o}C for 2 days. We found that only 34% of young and 12% of adult cold-induced genes were upregulated at both time points (Fig. 2.2A), which suggested that transcription in cold-activated iWAT is largely distinct between postnatal and adult animals. Gene ontology (GO) analysis of these subsets revealed that beta oxidation and tricarboxylic acid (TCA) cycle genes were upregulated at both time points (Fig. 2.2B), which was not surprising given their role in generating acetyl-CoA for the mitochondrial uncoupled respiration. Of note, cholesterol biosynthesis genes were selectively upregulated in p28-RT versus p28-30^{o}C iWAT, though their relevance to beiging is unclear.

Next, we identified the set of all genes that were differentially expressed in p28-RT versus 30^{o}C and plotted their expression across all four sets of samples. The resulting heatmap (Fig. 2.2C) showed that young cold- and warm-induced genes were in general not correlated with the corresponding conditions in adults. We observed a similar result when plotting expression of differentially expressed genes from the adult time point (Fig. 2.2D), reiterating that beige fat is transcriptionally distinct in young versus adult time points.

We next asked whether postnatal iWAT was epigenetically more similar to beige or to white fat in adults. To do this, we performed for ChIP-seq for H3K27ac, a marker of active chromatin, in iWAT from p28 and 9-wk-old mice housed at RT and identified two sets of peaks:

those that were enriched at p28 versus 9wks, and vice versa. When compared to preexisting lists of beige- or white-specific enhancers (Roh et al. 2018), we observed that young-associated peaks overlapped more strongly with the beige subset than the white (17.3% versus 2.2% respectively) (Fig. 2.2E). Conversely, adult-associated peaks overlapped more with the white subset than the beige (25.4% versus 0.7% respectively) (Fig. 2.2F). Thus, we concluded that young RT iWAT is epigenetically more similar to adult cold-induced beige fat, whereas adult RT iWAT resembles adult white fat.

SNS innervation of iWAT is dispensable for postnatal beiging.

To confirm that adrenergic signals were indeed dispensable for postnatal beiging, we used an orthogonal genetic approach of impairing sympathetic nervous system (SNS) innervation in iWAT, which activates the cold response in adults via the neurotransmitter norepinephrine (NE) (Cannon and Nedergaard 2011). We generated mice in which the neutrophin receptor TrkA (X. Chen et al. 2005) was deleted in cells expressing the SNS marker tyrosine hydroxylase (TH) (Jiang et al. 2017). We began by characterizing the extent of the deletion in iWAT. TH staining from p28 $TrkA^{Fl/+}Th^{Cre}$ control mice housed at RT showed that SNS innervation was uniformly distributed throughout the tissue, with no obvious correlation with the ING-DL asymmetry observed with UCP1 expression (Fig. 2.3A). Furthermore, homozygous-flox ($TrkA^{Fl/Fl}$) mice exhibited a significant reduction in SNS innervation even in the absence of Cre recombinase, which reflected the hypomorphic nature of this allele (X. Chen et al. 2005). The extant major nerve bundles were asymmetrically distributed towards the DL arm of the tissue, and the phenotype was even more severe in $TrkA^{Fl/Fl}Th^{Cre}$ tissue. This suggested that the SNS nerves normally originate from the dorsal root ganglion to which the DL arm is connected (W. Zeng et al. 2015; N. L. T. Nguyen et al. 2014). Furthermore, higher magnification images showed that whereas adipocytes in control iWAT were densely innervated by neurites,

these smaller branches were almost completely absent in homozygous $TrkA^{Fl/Fl}$ and $TrkA^{Fl/Fl}Th^{Cre}$ (henceforth collectively referred to as 'TrkA-KO') tissues (Fig. 2.3B).

We then proceeded to assess postnatal UCP1 expression in TrkA-KO tissues, and found that impairing SNS innervation had no effect on UCP1 expression (Fig. 2.3C-D). Furthermore, TrkA-KO mice that were born and housed at 30ºC also expressed similar levels of UCP1 compared to thermoneutral controls (Fig. 2.3E). Overall, we did not see any defect in either magnitude (Fig. 2.3F) or distribution of UCP1 expression in TrkA-KO iWAT. In addition, the observation that beiging is reduced with thermoneutral housing but not SNS-deficiency implies that the cold-response in postnatal iWAT is mediated by non-SNS signal(s).

Postnatal iWAT develops differently under thermoneutral versus SNS-deficient conditions.

We next sought to understand how TrkA-KO iWAT compares to normally-innervated tissue from mice housed at thermoneutrality at the transcriptional level, as both of these conditions resulted in loss of adrenergic signaling during development but had different effects on UCP1 expression. We performed RNA-seq on iWAT from p28 $TrkA^{Fl/Fl}Th^{Cre}$ mice housed at RT and compared this to the data sets previously analyzed in Fig. 2.2. Significantly more genes were downregulated in TrkA-KO iWAT than at thermoneutrality (404 and 210 respectively), but only 9.7% of these SNS-dependent genes were also upregulated at RT versus 30ºC (Fig. 2.4A), suggesting that the SNS's role in mediating the postnatal cold-response is part of a much broader portfolio. Indeed, GO analysis showed that the same pathways that fuel uncoupled respiration were downregulated in 30ºC but not TrkA-KO (Fig. 2.4B-C). In addition, steroid and cholesterol biosynthesis were selectively downregulated in TrkA-KO (Fig. 2.4D), though the 30ºC samples exhibited some (non-statistically-significant) downregulation as well. Cholesterol biosynthesis was upregulated by cold in young, but not adult, iWAT (Fig. 2.2B), though it is unclear if this is directly relevant to beige recruitment.

To achieve a better understanding of the interaction between the SNS innervation and ambient temperature, we performed the analysis for the complementary gene sets, i.e. genes that were upregulated at 30^{o}C versus those upregulated in TrkA-KO, finding that only 14.7% of the latter were sensitive to warming (Fig. 2.4E). GO analysis did not find any significantly enriched pathways within the 'up-in-TrkA-only' set, implying that the SNS does not repress any specific pathway (Fig. 2.4E). It did however reveal that muscle contraction genes were specifically elevated by warming, with a similar trend in TrkA-KO (Fig. 2.4G). It was recently shown that when subjected to cold stress, adipocytes in SNS-impaired iWAT can acquire glycolytic beige function via a myogenic intermediate state (Y. Chen et al. 2019). Hence this result suggests that SNS-independent beiging of postnatal iWAT may rely on such non-canonical pathways to achieve thermogenic capability.

Adrenergic signaling is absolutely required for adult cold-induced recruitment.

Given the unexpected results that postnatal beiging can occur in the absence of environmental cold and/or adrenergic signaling, we followed up on the role of the SNS in cold-challenged adult mice. We first verified the extent of SNS innervation impairment in adult TrkA-KO mice via TH staining and observed that the defect seen postnatally (Fig. 2.3A) persisted into adulthood. Next, we subjected adult TrkA-KO mice to cold challenge by housing them at 10^{o}C for 11 days. UCP1 staining in cleared iWAT from these mice showed a severe reduction in UCP1 expression in TrkA-KO iWAT, with TrkA$^{Fl/Fl}$ tissues exhibiting an intermediate defect between controls and TrkA$^{Fl/Fl}$Th^{Cre} (Fig. 2.5B-C). This was in line with previous findings that the SNS was indeed a critical mediator of cold-induced beiging in adult iWAT (Cannon and Nedergaard 2011; Nedergaard and Cannon 2014). Furthermore, the imaging also revealed that the UCP1+ adipocytes were located almost exclusively on the DL half of the iWAT, violating the ING > DL asymmetry seen under all other conditions. Given that the surviving SNS nerves are

also largely in the DL arm, this suggests that direct SNS signaling is required or cold-induced beiging in adult iWAT.

Finally, since SNS innervation is required for proper development of some tissue types (Borden et al. 2013), we asked whether constitutive impairment of innervation impaired the ability of TrkA-KO iWAT to respond to adrenergic signals. We used a pharmacological approach to address this question by injecting TrkA-KO adult mice with either the adrenergic agonist CL-316,243 or vehicle control for 7 consecutive days, and then harvested iWAT for UCP1 staining. We observed robust induction of UCP1 expression in both control and TrkA-KO iWAT, which confirmed that despite developing in the absence of proper SNS innervation, the ability of the adipocytes to respond to adrenergic signals remained intact in the adult time point (Fig. 2.5D-E).

DISCUSSION

Previous studies have described the temporal kinetics of postnatal beige fat induction (Odegaard et al. 2016; Y. Wang et al. 2017) while suggesting that this process is not entirely dependent on environmental cold (Chabowska-Kita et al. 2015; Chabowska-Kita and Kozak 2016). However, a thorough spatiotemporal characterization was not possible prior to the advent of techniques for 3D imaging of cleared adipose tissue (Chi et al. 2018). In this chapter we showed that beige fat induction follows a consistent spatial progression at both postnatal and adult time points. Given that reactivated postnatal beige adipocytes are a significant source of thermogenesis in adulthood (Y. Wang et al. 2017), one might assume that the beiging process is governed by the same set of principles at both time points. Contrary to this expectation, we found that postnatal beiging occurs even in the absence of environmental cold or adrenergic signaling, both of which are essential in the adult response. One possible explanation is that since the beiging process takes time, having a constitutive basal level of

thermogenic capacity would allow young animals to tolerate sudden fluctuations in ambient temperature. Ultimately, environmental cold was associated with distinct transcriptional profiles in postnatal versus adult iWAT, thereby reiterating that the tissue is fundamentally different at these two time points.

We also showed that although the SNS is not required for expression of UCP1 and thermogenic pathways such as beta oxidation, it positively regulates genes involved in synthesis of sterol metabolites such as cholesterol and mevalonate. Notably, the latter is involved in lipid homeostasis in WAT (Yeh et al. 2018), as well as beiging in adult mice and humans (Balaz et al. 2019), suggesting that the SNS might contribute to beiging in other indirect ways besides activating UCP1 expression itself. Crucially, adult SNS-deficient iWAT could induce UCP1 in response to the adrenergic agonist CL-316,243, and thus the SNS is not required for licensing of thermogenic capability during development.

The amplitude of the postnatal beiging response is increased under colder housing conditions, implying that it is regulated by both temperature-sensitive and -insensitive signals. This model immediately suggests two lines of inquiry. Firstly, as SNS-deficiency does not phenocopy thermoneutral housing conditions, what are the non-adrenergic mediators of the temperature-sensitive response? Secondly, what are the tissue- or cell-intrinsic signals that drive postnatal beiging independently of environmental conditions? The identification of these two sets of signals will improve our understanding of the postnatal beiging process and its implications for the adult cold response. One potential approach for future studies could be to follow up on strain-intrinsic differences, e.g. 129/SvEv having increased postnatal beiging capacity compared to C57BL/6J (Gouon-Evans and Pollard 2002; Lasar et al. 2013).

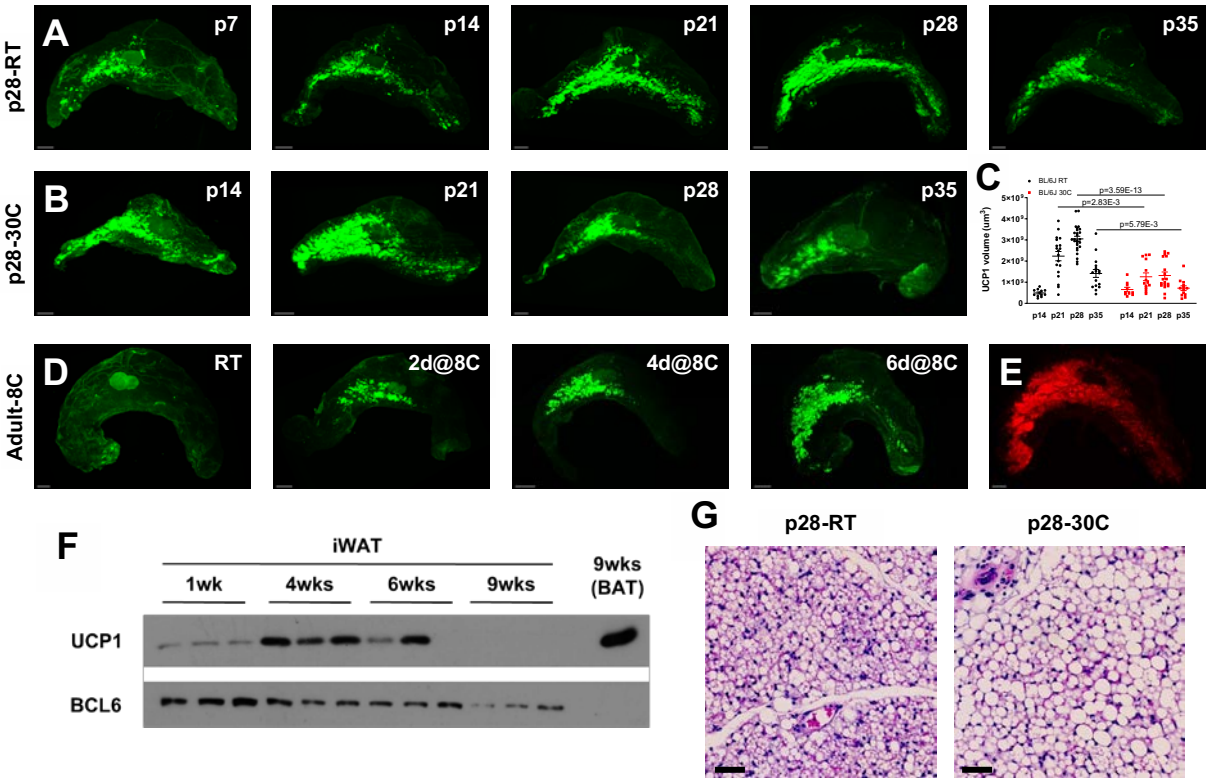

Figure 2.1: Beiging follows a fixed spatiotemporal pattern in both young and adult iWAT.

(A) Representative whole tissue uncoupled protein 1 (UCP1) staining of cleared inguinal white adipose tissue (iWAT) from young BL/6J mice housed at room temperature (RT) (scale bar = 1 mm). (B) UCP1 staining of iWAT from young BL/6J mice housed at 30°C (scale bar = 1 mm). (C) Quantification of UCP1 staining in (A) and (B) using Imaris software. (D) UCP1 staining of iWAT from 14-15 wk old BL/6J mice housed at RT or 8°C for 2-6 days (scale bar = 1 mm). (E) RFP staining of iWAT from 20-wk-old CAG-LSL-tomato Ucp1^{Cre-} mice housed at RT (scale bar = 1 mm). (F) Western blot of iWAT UCP1 from BL/6J mice housed at RT. (G) Representative H&E stain of iWAT from p28 BL/6J mice housed at RT (scale bar = 50 μm).

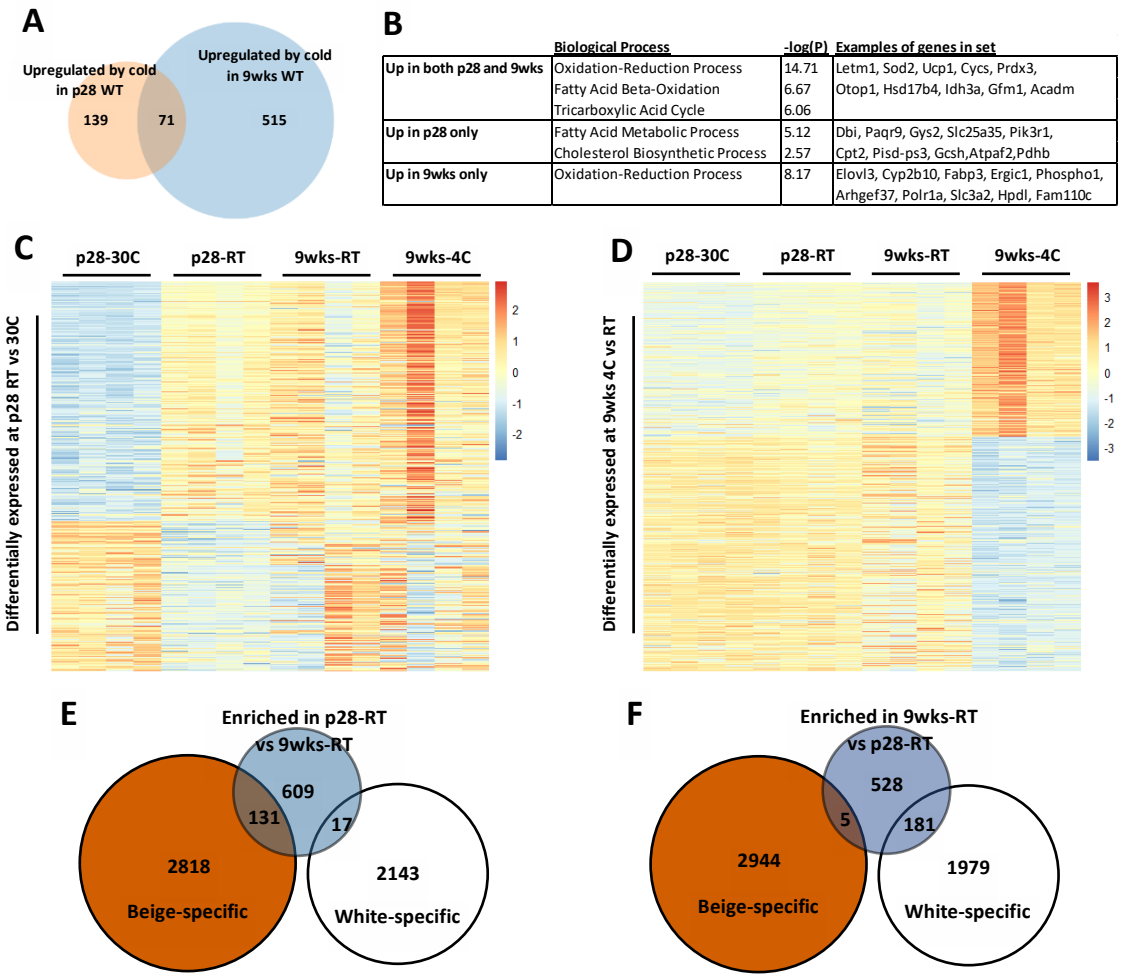

	Biological Process	-log(P)	Examples of genes in set
Up in both p28 and 9wks	Oxidation-Reduction Process	14.71	Letm1, Sod2, Ucp1, Cycs, Prdx3,
	Fatty Acid Beta-Oxidation	6.67	Otop1, Hsd17b4, Idh3a, Gfm1, Acadm
	Tricarboxylic Acid Cycle	6.06	
Up in p28 only	Fatty Acid Metabolic Process	5.12	Dbi, Paqr9, Gys2, Slc25a35, Pik3r1,
	Cholesterol Biosynthetic Process	2.57	Cpt2, Pisd-ps3, Gcsh,Atpaf2,Pdhb
Up in 9wks only	Oxidation-Reduction Process	8.17	Elovl3, Cyp2b10, Fabp3, Ergic1, Phospho1, Arhgef37, Polr1a, Slc3a2, Hpdl, Fam110c

Figure 2.2: Young and adult beige fat are transcriptionally and epigenetically distinct.

(A) Comparison of young- and adult-cold-dependent genes (RNA-seq; n=4 per group). (B) Gene ontology (GO) analysis of enriched pathways (FDR ≤ 0.05) and top 10 genes (fold change ≥1.5 and p-adj ≤0.05) per set in (A). (C) Expression of all young-cold-dependent genes compared across young and adult time points. (D) Same as (C), but for adult-cold-dependent genes. (E) Venn diagram comparing H3K27ac peaks enriched in young RT over adult RT iWAT with beige- and white-specific enhancers (ChIP-seq; n=3 per group). (F) Same as (E) but with peaks enriched in adult RT over young RT iWAT.

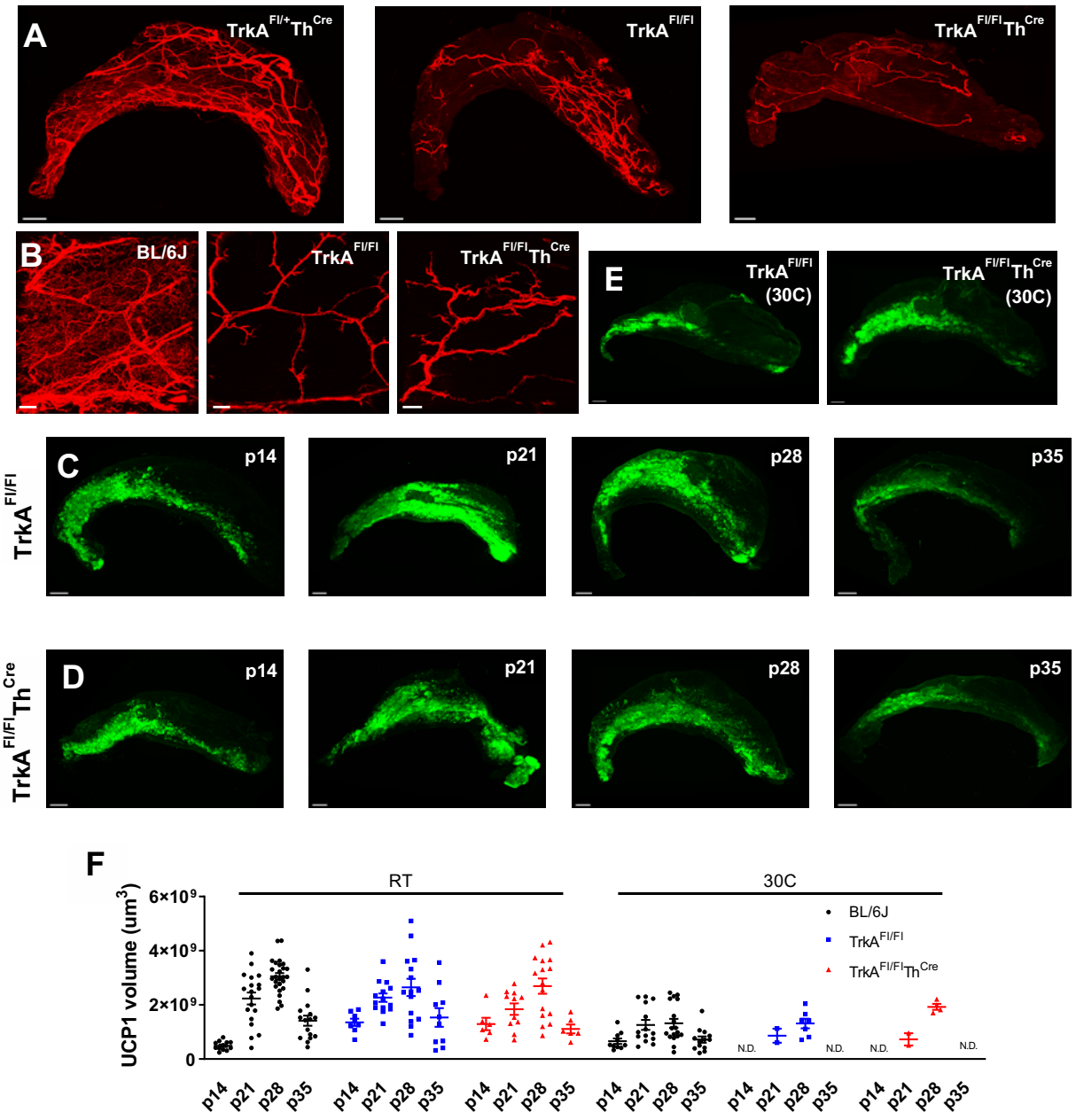

Figure 2.3: SNS innervation of iWAT is dispensable for postnatal beiging.

(A) Representative whole tissue tyrosine hydroxylase (TH) staining of iWAT from p28 control and TrkA-KO mice housed at RT (scale bar = 1 mm). (B) High magnification zooms of iWAT from p28 control and TrkA-KO mice housed at RT (scale bar = 200 μm). (C) UCP1 staining of iWAT from $TrkA^{Fl/Fl}$ mice housed at RT (scale bar = 1 mm). (D) Same as (C) but with $TrkA^{Fl/Fl}Th^{Cre}$ mice. (E) UCP1 staining of iWAT from p28 TrkA-KO mice housed at 30°C (scale bar = 1 mm). (F) Quantification of UCP1 staining in (C)-(E), inc. data from Fig. 2.1 (A)-(C).

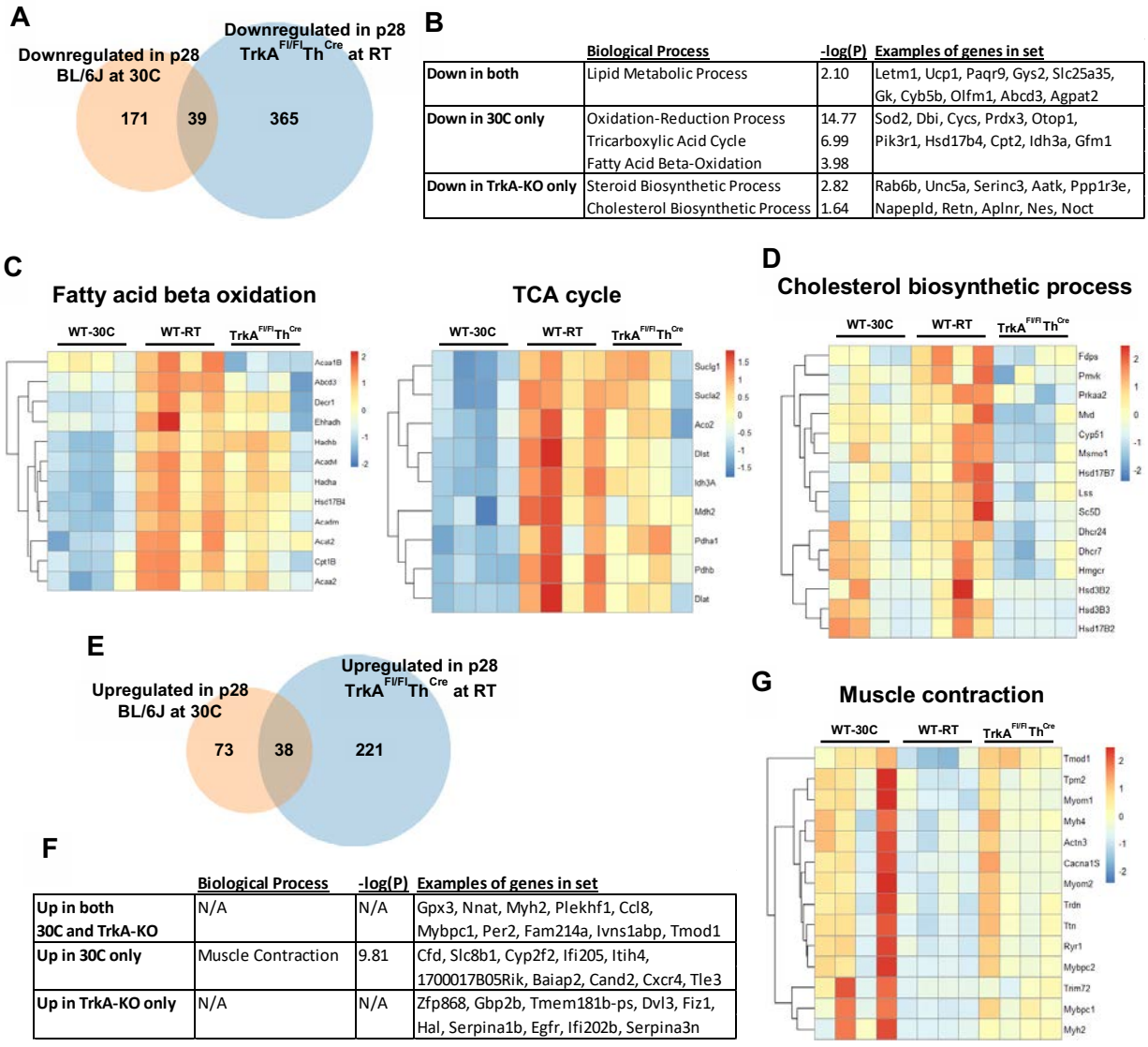

	Biological Process	-log(P)	Examples of genes in set
Down in both	Lipid Metabolic Process	2.10	Letm1, Ucp1, Paqr9, Gys2, Slc25a35, Gk, Cyb5b, Olfm1, Abcd3, Agpat2
Down in 30C only	Oxidation-Reduction Process	14.77	Sod2, Dbi, Cycs, Prdx3, Otop1,
	Tricarboxylic Acid Cycle	6.99	Pik3r1, Hsd17b4, Cpt2, Idh3a, Gfm1
	Fatty Acid Beta-Oxidation	3.98	
Down in TrkA-KO only	Steroid Biosynthetic Process	2.82	Rab6b, Unc5a, Serinc3, Aatk, Ppp1r3e,
	Cholesterol Biosynthetic Process	1.64	Napepld, Retn, Aplnr, Nes, Noct

	Biological Process	-log(P)	Examples of genes in set
Up in both 30C and TrkA-KO	N/A	N/A	Gpx3, Nnat, Myh2, Plekhf1, Ccl8, Mybpc1, Per2, Fam214a, Ivns1abp, Tmod1
Up in 30C only	Muscle Contraction	9.81	Cfd, Slc8b1, Cyp2f2, Ifi205, Itih4, 1700017B05Rik, Baiap2, Cand2, Cxcr4, Tle3
Up in TrkA-KO only	N/A	N/A	Zfp868, Gbp2b, Tmem181b-ps, Dvl3, Fiz1, Hal, Serpina1b, Egfr, Ifi202b, Serpina3n

Figure 2.4: Postnatal iWAT develops differently under thermoneutral versus SNS-deficient conditions.

(A) Venn diagram of RNA-seq data comparing cold-dependent and SNS-dependent genes in iWAT from p28 mice (n=4 per group). (B) GO analysis of enriched pathways (FDR ≤ 0.05) and top 10 genes (fold change ≥1.5 and p-adj ≤0.05) per set in (A). (C) Expressions of pathways downregulated in 30°C but not TrkA$^{Fl/Fl}$Th^{Cre} iWAT. (D) Expression of 'cholesterol biosynthetic process' pathway downregulated in TrkA$^{Fl/Fl}$Th^{Cre} iWAT but not 30°C. (E) Venn diagram comparing warm-induced genes and genes upregulated in TrkA$^{Fl/Fl}$Th^{Cre} iWAT. (F) GO analysis of enriched pathways (FDR ≤ 0.05) and top 10 genes (fold change ≥1.5 and p-adj ≤0.05) per set in (E). (G). Expression of 'muscle contraction' pathway upregulated in 30°C iWAT.

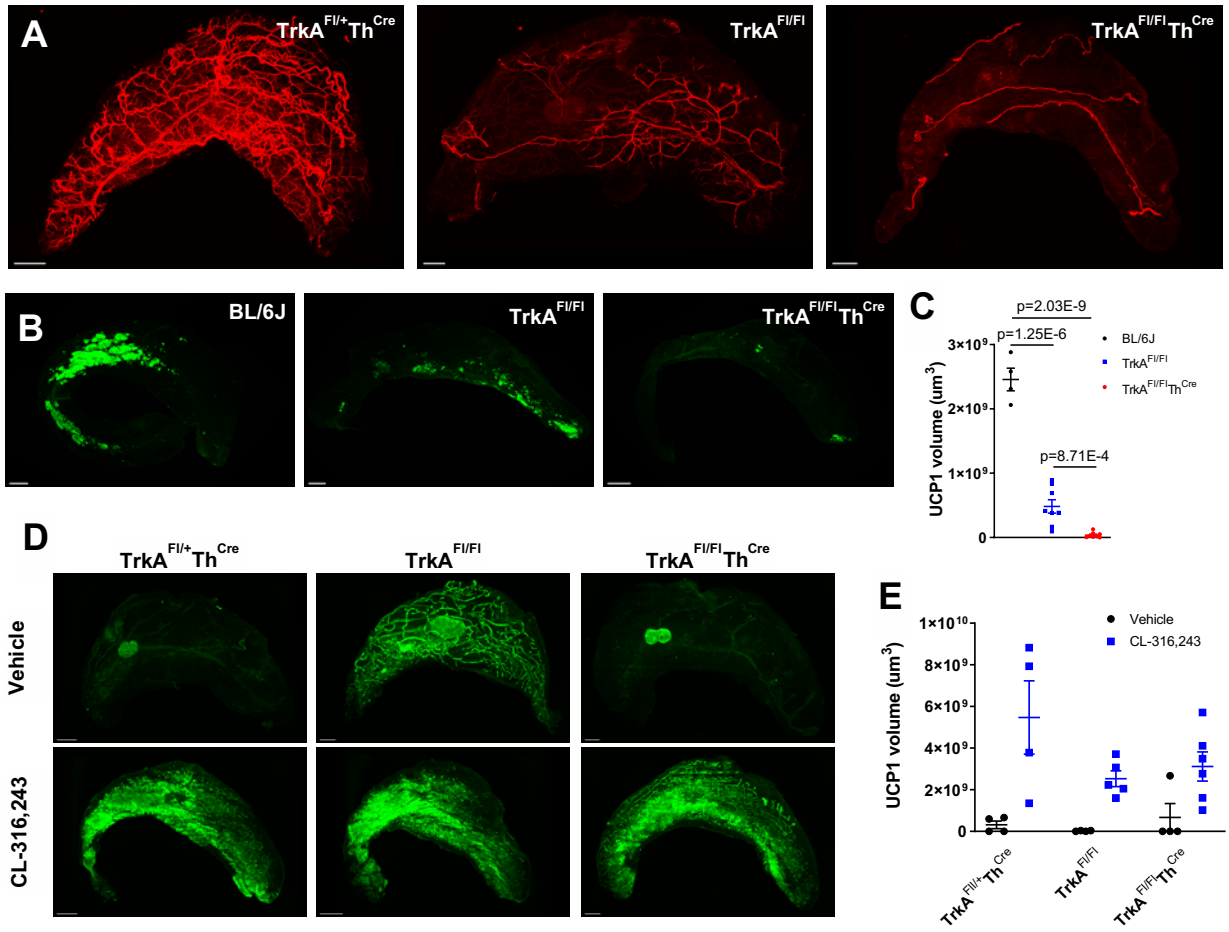

Figure 2.5: Adrenergic signaling is absolutely required for adult cold-induced recruitment.

(A) Representative whole tissue TH staining of iWAT from 8-10 wk old TrkA-KO mice housed at RT (scale bar = 1 mm). (B) UCP1 staining of iWAT from 14-15 wk old TrkA-KO mice housed at 10°C for 11 days (scale bar = 1 mm). (C) Quantification of UCP1 staining in (B). (D) UCP1 staining of iWAT from 10-11 wk old TrkA-KO mice treated daily with either vehicle or 1 mg/kg CL-316,243 I.P. for 7 days at RT (scale bar = 1 mm). (E) Quantification of UCP1 staining in (D).

METHODS

Mice

All animal studies were conducted under an approved Institutional Animal Care and Use Committee (IACUC) protocol at University of California, San Francisco (UCSF). All mice were congenic to the C57BL6/J background and housed in the mouse vivarium at ambient temperatures ranging between 4°C or 30°C as indicated. A 12-hour light:dark cycle was used, and food and water were available *ad libitum*. For room temperature (RT) housing, mouse cages were placed on racks exposed to the room atmosphere (~22°C). For housing at other temperatures, cages were placed in temperature-controlled chambers (Darwin Chambers or Power Scientific) set to the desired value. Unless otherwise indicated, mice were housed at a constant temperature from birth.

Cold tolerance tests were performed as described previously (Lee et al., 2015). Briefly, two mice were housed in each pre-chilled cage with food and water available *ad libitum*. Rectal temperature was measured hourly using a BAT-12 microprobe thermometer with RET-3 thermocouple (PhysiTemp). Per IACUC guidelines, survival was defined as a core temperature > 28°C. Similar housing conditions were used for 48-hour cold exposure studies.

Mice were fed normal chow diet (5053, Pico labs). Both male and female mice were used for all experiments (see figure legends for exact ages). C57BL/6J, Th^{Cre}, and CAG-LSL-tomato mice were purchased from Jackson Laboratories and bred in our vivarium. $Trka^{Fl/Fl}$ mice were graciously shared with us by Rejji Kuruvilla at Johns Hopkins University. For all *in vivo* studies, cohorts of at least three mice per genotype or treatment group were used, and experiments were repeated two or three times independently.

Methods Details:

Tissue Clearing:

Inguinal white adipose tissue (iWAT) samples were processed using the recently published Adipo-Clear protocol (Chi et al., 2018). Briefly, samples were fixed overnight in 4% PFA, washed in PBS, and dehydrated via methanol gradient. They were then delipidated using dichloromethane (DCM), bleached in a hydrogen peroxide-DMSO solution overnight, and rehydrated via methanol gradient. Samples were incubated with primary followed by secondary antibodies (37^{o}C for 3 days each), with wash steps after each stain (see STAR Methods for full list of antibodies). Finally, they were dehydrated via methanol series, delipidated with DCM, then cleared in dibenzyl ether (DBE). All steps apart from antibody staining were carried out at RT with shaking.

3D Imaging:

Cleared samples were imaged on a Nikon AZ100 microscope that had been modified for light sheet imaging (UCSF Nikon Imaging Center), in conjunction with Micro-Manager software (https://micro-manager.org). Acquisition settings for whole-tissue and high-magnification zoomed shots were 1x objective / 10um step-size and 5x objective / 3um step-size respectively.

Image Processing and Quantification:

All 3D images were processed using Imaris x64 software (version 9.3.1, Bitplane), 2D snapshots taken using the snapshot function. For UCP1 volume quantification, the Surface tool was used to generate a mask of the UCP1-positive region, followed by automated calculation of the volume by the software.

Histology:

Freshly isolated iWAT was fixed in 10% formalin, and then submitted for embedding, sectioning,

and H&E staining at the UCSF Liver Center Pathology and Imaging Core in partnership with the Peninsular Histopathology Laboratory. H&E slides were scanned using an Axio Scan.Z1 (Zeiss).

RNA Isolation:

Snap-frozen iWAT samples were homogenized in Trisure (Bioline) using a TissueLyser II (Qiagen) for 2 minutes at 30 Hz. Phase separation was induced with 1-Bromo-3-chloropropane, followed by precipitation in isopropanol and two 70% ethanol washes. RNA concentration was measured with a Nanodrop 2000 spectrophotometer (Thermo Fisher Scientific).

Chromatin Immunoprecipitation:

Anti-H3K27ac chromatin immunoprecipitation was performed in isolated iWAT samples as described previously (Kutyavin and Chawla 2019). Briefly, frozen samples were minced and fixed in 1% formaldehyde in PBS for 20 min at room temperature, followed by addition of 125 mM glycine. Next, chromatin was extracted via nuclear isolation, lysis, and sonication. Chromatin samples were incubated with 2 µg of anti-H3K27ac antibody (Abcam #ab4729) overnight at 4°C, then with 50 µl of Protein G Dynabeads for 4 hours at 4°C. Following multiple wash steps, the beads were resuspended in elution buffer (50 mm Tris-Cl, pH 8.0, 10 mm EDTA, 1% SDS) and incubated at 65^{o}C for 10 mins. The supernatant was collected and incubated at 65^{o}C overnight to reverse crosslinks. Samples were treated with RNAse cocktail (Invitrogen #AM2286, 1 hour at 37°C), Proteinase K (Promega #V302B, 2 hours at 65°C), and DNA was isolated with a Qiaquick PCR Purification Kit (Qiagen) according to the manufacturer's instructions. DNA concentrations were measured with a Qubit dsDNA High Sensitivity Assay Kit and a Qubit 2.0 fluorimeter (Thermo Fisher Scientific).

Sequencing Library Preparation:

RNA-Seq libraries were constructed as described previously (Kutyavin and Chawla 2019). Briefly, the TruSeq Stranded mRNA Library Prep Kit (Illumina) was used according to the manufacturer's instructions with 2 µg of total RNA was used as the starting material. PolyA-

containing RNA was purified and fragmented, followed by first and second strand cDNA synthesis, adapter ligation, and PCR amplification (15 cycles). A library size of 200-300 bp was verified by agarose gel electrophoresis and library concentration was measured with a Qubit dsDNA High Sensitivity Assay Kit and a Qubit 2.0 fluorimeter (Thermo Fisher Scientific). For construction of ChIP-Seq libraries, the same kit was used with several modifications. 10 ng of ChIP DNA was used as input and treated with end repair enzymes (Thermo Fisher Scientific #K0771) before proceeding to the 3' adenylation and adapter ligation steps. Subsequently, samples were resolved on a 2% agarose gel containing SYBR Gold Stain (Life Technologies # S11494), visualized by ultraviolet illumination, and gel sections containing 250-500 bp fragments were excised and DNA extracted with a Gel DNA Recovery Kit (Zymo Research # D4007). Libraries were then amplified by PCR and quantified as described above.

Next Generation Sequencing:

Pooled library samples were diluted to 10 nM concentration and submitted to the UCSF CAT Core for sequencing on a HiSeq 4000 (single-read mode).

RNA-seq Analysis:

Analysis was performed as described previously (Kutyavin and Chawla 2019). Briefly, raw sequence data were pseudo-aligned to the mouse transcriptome (mm10, UCSC annotation) using Kallisto. Differential expression was defined as a fold change ≥1.5 and an adjusted p-value ≤0.05 and calculated using DESeq2. Heat maps were generated in R. Venn Diagrams were generated using BioVenn (https://www.biovenn.nl) and Venn Diagram Generator (https://academo.org/demos/venn-diagram-generator/). Gene ontology enrichment analysis was performed using DAVID Bioinformatics Resources 6.8.

ChIP-seq Analysis:

Analysis was performed as described previously (Kutyavin and Chawla 2019). Briefly, raw

sequence data were aligned to the mouse genome (mm10) using Bowtie2. Homer was used to identify and annotate H3K27ac peaks in 3 biological replicates per condition. Differential H3K27ac abundance was defined as a fold change ≥2 and an adjusted p-value ≤0.05. Homer was also used for sequence motif enrichment analysis. DeepTools was used to generate heat maps of differentially abundant peaks. BigWig files were generated with the bedGraphToBigWig program and visualized with the UCSC Genome Browser.

For analysis of brown and white adipocyte-specific enhancers, the coordinates of previously characterized adipocyte H3K27ac and H3K4me1 peaks were obtained from the laboratory of Dr. Evan Rosen (Roh et al. 2018), and H3K27ac ChIP-seq data for beige and white adipocytes (in warmth-adapted mice) were downloaded from Sequence Read Archive (SRA) (#SRP126748). We defined active enhancers as H3K27ac peaks that overlap at least one H3K4me1 peak, as determined by BEDtools. Active enhancers were classified as beige or white adipocyte-specific if they had 4-fold or greater enrichment of H3K27ac in the corresponding cell type (relative to the other), as determined by DESeq2 (adjusted p-value ≤0.05).

β3-adrenergic Signaling:

For *in vivo* activation of β3-adrenergic signaling, mice housed at RT were given an intraperitoneal injection of CL-316243 (1 mg/kg in saline) for seven consecutive days, followed by iWAT isolation for clearing and imaging.

Tissue Oxygen Consumption:

Oxygen consumption measurement was performed as described previously (Kutyavin and Chawla 2019). Briefly, freshly isolated iWAT and BAT were finely minced, and the fragments resuspended in respiration buffer (PBS containing 20 mg/ml BSA, 25 mM glucose, and 1 mM pyruvate). The rate of oxygen consumption was recorded with a Mitocell S200 respirometry system (Strathkelvin Instruments). Data were analyzed with Strathkelvin 782 Oxygen System software (version 4.1).

Immunoblotting:

Western blotting for UCP1 and BCL6 was performed as described previously (Kutyavin and Chawla 2019). To prepare whole cell extracts, frozen tissue samples were placed into 2 mL tubes containing 0.5 mL of modified RIPA buffer (50 mM Tris-Cl, pH 7.5, 150 mM NaCl, 1% Nonidet P-40 substitute (Fluka), 0.1% SDS, 0.5% sodium deoxycholate, 1 mM EDTA, with 1:200 protease inhibitor cocktail (Sigma-Aldrich #P8340) and a metal bead, and homogenized in a TissueLyser II (Qiagen) for 120 seconds at 30 Hz. Nuclear extracts were prepared using NE-PER Nuclear and Cytoplasmic Extraction Reagents (Thermo Fisher Scientific #78833) according to the manufacturer's instructions. Protein concentration was measured with a Pierce BCA Protein Assay Kit (Thermo Fisher Scientific #23225) according to the manufacturer's instructions. Protein (5-30 µg) was diluted in sample buffer (62.5 mM Tris-Cl, pH 6.8, 10% glycerol, 2% SDS, 5% 2-mercaptoethanol, 0.008% bromophenol blue), incubated at 90° C for 5 minutes, separated by SDS–PAGE, and transferred to a 0.45 µm nitrocellulose membrane (Bio-Rad #1620115). The membrane was blocked with 5% nonfat dry milk in PBS containing 0.1% Tween-20 for 30 mins and probed with the primary and HRP-conjugated secondary antibodies diluted in PBS containing 0.1% Tween-20 and 2% BSA (see STAR Methods for full list of antibodies). HSP90a/b and Lamin B1 were used as loading controls for whole cell extracts and nuclear extracts, respectively. Immunoblotted proteins were detected on HyBlot CL autoradiography film (Denville Scientific #1159M39) using ProSignal Pico chemiluminescent substrate (Prometheus Protein Biology Products #20-300) and Mini-Medical 90 X-ray Film 27 Processor (AFP Imaging #9992305300).

Chapter 3 :

BCL6 and type 2 cytokines play complex roles in beiging

No one really knows how the game is played.

The art of the trade, how the sausage gets made.

—Lin-Manuel Miranda, *Hamilton: An American Musical*

ABSTRACT

Postnatal beige fat in inguinal white adipose tissue (iWAT) develops even in the absence of environmental cold or adrenergic signaling, which implies the existence of tissue- or cell-intrinsic signals that encode the beiging process. However, the identity of these signals remains unclear. Here we used light sheet microscopy and RNA sequencing to show that postnatal beiging was significantly abrogated in mice lacking either B-cell lymphoma 6 (BCL6) in adipocytes or the cytokines interleukin (IL)-4 and -13; these signaling pathways also contributed to cold-induced beiging in adult animals to varying degrees. Together these findings identify BCL6 and type 2 cytokines as cell- and tissue-intrinsic drivers of beiging in postnatal and adult iWAT respectively.

INTRODUCTION

Endothermic organisms such as mammals rely on internal physiological processes to regulate their body temperature in the face of fluctuations in environmental conditions. Uncoupled respiration in brown and beige adipocytes is a major source of thermogenesis; in particular, the latter is inducible by cold stress in adult animals (Cannon and Nedergaard 2004). Previous work has shown that postnatal beiging occurs even under thermoneutral or SNS-impaired conditions (Chabowska-Kita et al. 2015; Odegaard et al. 2016, Chapter 2 of this dissertation), which is counter-intuitive given that this process presumably evolved to protect young animals from thermal stress (Chabowska-Kita and Kozak 2016). This raises the question of what signals are actually required for beiging in postnatal animals.

Two potential candidates are the transcriptional repressor B-cell lymphoma 6 (BCL6) and type 2 immune cytokine signaling. The former was originally identified as a regulator of T follicular helper (T_{FH}) and germinal center (GC) B cells (Johnston et al. 2009; Bélanger and Crotty 2016), and was been recently implicated in the maintenance of both brown and white adipose tissue homeostasis (Senagolage et al. 2018; Kutyavin and Chawla 2019). The latter consists of the cytokines interleukin-4 (IL-4), IL-5, and IL-13, which are secreted by type 2 innate lymphoid cells (ILC2s) and eosinophils as part of an immune signaling cascade, and play varied roles in postnatal licensing of thermogenic function (Odegaard et al. 2016) and cold-induced beiging (K. D. Nguyen et al. 2011; Qiu et al. 2014; M.-W. Lee et al. 2014; Brestoff et al. 2014) in inguinal white adipose tissue (iWAT).

Here, we investigated the role of BCL6 and immune cytokine signaling in beige fat recruitment in both postnatal and adult settings. We found that deletion of BCL6 with a pan-adipocyte Cre recombinase completely abrogated UCP1 expression in both postnatal and adult time points, whereas deletion with Ucp1-cre (i.e. after UCP1 had been expressed) did not show a significant defect. These results suggest that BCL6 is required for *de novo* differentiation of

precursors into beige adipocytes but is required for neither transdifferentiation of naïve white adipocytes, nor reactivation of ex-UCP1^{+} adipocytes in adult iWAT. In addition, cytokine-knockout mice exhibited defective beiging in both postnatal and adult iWAT, suggesting that these immune signals are important throughout the animal's lifetime. In conclusion, this chapter identifies roles for cell-intrinsic (BCL6) and tissue-intrinsic (type 2 cytokines) signals that drive temperature-independent beige fat recruitment in postnatal iWAT.

RESULTS

Adipocyte BCL6 is required for postnatal beiging but regulates distinct transcriptional pathways from cold-induced beige.

As our previous findings showed that postnatal beige fat development occurs even in the absence of environmental cold and adrenergic signaling (Chapter 2 of this dissertation), we sought to identify other signaling pathways that contributed to this process. One candidate was B-cell lymphoma 6 (BCL6), a transcriptional repressor that was recently shown to play a role in brown and white adipose tissue metabolism (Senagolage et al. 2018; Kutyavin and Chawla 2019). We began by quantifying expression of BCL6 protein in inguinal white adipose tissue (iWAT) of BL/6J mice housed at room temperature (RT), and found that it was strongly expressed throughout the postnatal period and decayed as the animals matured into adulthood (Fig. 3.1A), i.e. BCL6 and UCP1 expression have similar kinetics in postnatal iWAT (Fig. 2.1F).

To selectively delete Bcl6 expression in iWAT adipocytes, we generated 'Prx-cre' mice by crossing Bcl6$^{Fl/Fl}$ (Kaji et al. 2012; Hollister et al. 2013) to paired related homeobox transcription factor 1 (Prx1)-Cre, which exhibits recombinase activity in adipocyte precursors in subcutaneous WAT (Sanchez-Gurmaches, Hsiao, and Guertin 2015). Hematoxylin and eosin (H&E) staining of iWAT from p28 Prx-cre mice housed at RT showed a significant reduction in

beige adipocyte morphology compared to littermate controls (Fig. 3.1B). We then stained for uncoupled protein 1 (UCP1) in whole cleared iWAT from p28 Prx-cre mice, and observed a near complete loss of UCP1 expression in these postnatal tissues (Fig. 3.1C-D). To confirm this result independently, we crossed $Bcl6^{Fl/Fl}$ and adiponectin (AdipoQ)-Cre lines to generate AdipoQ-cre mice, which excise Bcl6 during adipocyte differentiation (Berry and Rodeheffer 2013). We observed a similar defect in p28 AdipoQ-cre iWAT (Fig. 3.1E-F), thus confirming that BCL6 plays a critical role in postnatal beiging.

We next asked whether loss of BCL6 (and by extension UCP1) in adipocytes in iWAT resulted in defective thermogenic function by measuring the oxygen consumption rate of iWAT adipocytes from p28-KO mice housed at RT. We observed a moderate defect in respiratory activity in iWAT (Fig. 3.1G), but not in interscapular BAT (iBAT) from the same animals (Fig. 3.1H) which does not exhibit $Prx1^{Cre}$ recombinase activity (Sanchez-Gurmaches, Hsiao, and Guertin 2015). Furthermore, when we subjected p28 Prx-cre mice to acute 4°C cold challenge, they showed significantly impaired cold tolerance relative to controls as measured by body temperature and survival rate (Fig. 3.1I-J). This result also suggests that subcutaneous beige fat (which encompasses iWAT) contributes significantly to the organism's cold tolerance, despite having a lower weight-normalized respiratory rate than iBAT.

Next, we sought to understand BCL6's role in iWAT at the transcriptional level via RNA-seq of p25 Prx-cre mice housed at RT and found that lipid and carbohydrate metabolic pathways were downregulated in Prx-cre compared to controls, whereas no one pathway was significantly upregulated (Figs. 3.1K-L). We then compared the set of genes downregulated in Prx-cre to the set of cold-dependent genes (Fig. 2.2) and found that only 19.8% of BCL6-dependent genes were induced by cold (Fig. 3.1M). Gene ontology (GO) analysis of these subsets showed that BCL6 was specifically required for fatty acid, but not carbohydrate,

metabolic pathways (Fig. 3.1N). Together, these results suggest that BCL6 is required for the expression of both UCP1 and the metabolic pathways that fuel its thermogenic activity.

BCL6 is required for cold-induced beiging in adults, but not reactivation of dormant adipocytes.

Given the severe defect in beiging in Prx-cre mice at the postnatal time point, we wanted to ask whether BCL6 continued to play a role in adult iWAT. UCP1 staining of iWAT from Prx-cre mice housed at 4^{o}C for 2 days showed a near complete absence of UCP1 expression (Fig. 3.2A-B), whereas cold-challenged AdipoQ-cre mice only exhibited a partial defect (Fig. 3.2C-D). This difference could be explained by AdipoQ-cre only targeting mature (i.e. differentiated) adipocytes in adult mice, whereas Prx1-cre acts earlier at the precursor stage (Sanchez-Gurmaches, Hsiao, and Guertin 2015). By extension, this implies that in adults BCL6 is important for early differentiation of adipocyte precursors, but may play a smaller role in the transdifferentiation of mature white adipocytes.

As the sympathetic nervous system (SNS) plays a key role in adult beiging (Cannon and Nedergaard 2011), we asked whether innervation was impaired in iWAT from adult Prx-cre mice. TH staining did not reveal any noticeable differences in SNS innervation between Prx-cre and controls (Fig. 3.2E), thus ruling this out as an explanation for the defect seen in Figs. 3.2A-B. We then asked whether the defect in cold-induced UCP1 expression resulted in defective respiratory capacity. Indeed, the oxygen consumption rate of iWAT from adult Prx-cre mice housed at 4^{o}C was significantly reduced compared to controls, whereas iBAT was unimpaired (Figs. 3.2F-G).

We then sought to characterize BCL6's role in the adult cold response at the transcriptional level by performing RNA-seq on iWAT from adult Prx-cre mice housed at 4°C for 2 days. GO analysis showed that, as in postnatal iWAT (Fig. 3.1K), loss of BCL6 in adult iWAT resulted in defective transcription of lipid metabolism and beta oxidation genes (Fig. 3.2H). However, whereas no specific pathways were significantly upregulated in postnatal Prx-cre iWAT, expression of various pathways such as cell adhesion were increased in the absence of BCL6 at the adult time point (Fig. 3.2H).

Since both Prx1-Cre and AdipoQ-Cre recombinases are active throughout the animals' lifetime, and that ex-UCP1-expressing adipocytes remained dormant into adulthood (Fig. 2.1E), it is not possible to discriminate between BCL6's contribution to thermogenesis at either time point using these models. Thus, we generated $Bcl6^{Fl/Fl}Ucp1^{Cre}$ (Ucp1-cre) mice which excise Bcl6 only in cells with prior history of UCP1 expression (i.e. postnatally). We began by evaluating UCP1 expression in iWAT from p28 Ucp1-cre mice housed at RT and found that there was no defect at this time point (Fig. 3.2I-J), which was expected given the timing of the deletion. We then assessed UCP1 expression in iWAT from adult Ucp1-cre mice housed at 4°C for 2 days and did not observe a statistically significant difference in Ucp1-cre compared to controls (Fig. 3.2K-L). This implies that BCL6 is not required for maintenance of beige potential in adipocytes that had expressed UCP1 postnatally and by extension, that it is primarily required for *de novo* differentiation of beige adipocytes in adult iWAT.

To verify this result, we performed RNA-seq on adult Ucp1-cre mice that had been housed at 4°C for 2 days and compared it to the previously analyzed cold-induced Prx-cre data sets (young and adult). We identified the set of genes that were differentially expressed in young Prx-cre, plotted their expression across all three groups, and found that while cold-induced transcription was broadly similar in young and adult Prx-cre iWAT, there was no difference between Ucp1-cre and controls (Fig. 3.2M). In fact, a total of only 5 genes were

differentially expressed between Ucp1-cre and control iWAT (data not shown), which supported the conclusion that adipocytes require BCL6 before, but not after, they have expressed UCP1. Finally, to check that Bcl6 excision had indeed occurred in these sequenced samples, we analyzed the *Bcl6* locus in the UCSC Genome Browser and observed moderate reduction in peaks corresponding to the targeted exons 7-9 (Hollister et al. 2013) (Fig. 3.2N). This confirmed that *Bcl6* had been excised in a large proportion of adipocytes without having a significant impact on the overall transcriptional profile of the iWAT upon cold challenge.

Immune signals play complicated roles in postnatal and adult beiging.

Previous studies have established the role of type 2 immune cytokine signaling in driving the adult cold response (Qiu et al. 2014; M.-W. Lee et al. 2014), as well as a distinct role for interleukin (IL)-33 in thermogenic licensing of beige adipocytes during development (Odegaard et al. 2016). As the type 2 cytokines IL-4 and -13 lie downstream of the IL-33 signaling cascade (McCormick and Heller 2015), we sought to investigate whether these signals contribute to postnatal beiging. UCP1 staining in iWAT from postnatal IL13-KO and IL4/13-double knockout ("IL4/13-DKO") mice showed reductions in peak (p28) UCP1 expression at RT, relative to congenic wild-type (WT) controls (Figs. 3.3A-B). However, no defect was observed in IL4Ra-KO mice from both BL/6J and BALB/cJ backgrounds, even though both IL-4 and IL-13 canonically signal through this receptor subunit (McCormick and Heller 2015).

To verify this contradictory result, we analyzed iWAT from mice lacking signal transducer and activator of transcription 6 (STAT6), a key downstream signaling protein from IL-4R (McCormick and Heller 2015), and found no defect in iWAT UCP1 from p28 mice of either background at RT (data not shown). Finally, we also observed stronger peak UCP1 expression in BALB/cJ versus BL/6J mice (Fig. 3.3B), which is congruent with the paradigm of mice from these strains skewing towards Type 2 and Type 1 immune responses respectively (Spellberg and Edwards 2001).

Given that postnatal UCP1 expression was partially reduced in IL4/13-DKO mice housed at RT and in WT mice housed at thermoneutrality (Fig. 1.1C), we asked if combining the two conditions would result in a cumulative defect. Indeed, UCP1 expression in iWAT from IL4/13-DKO mice housed at 30^{o}C failed to increase between p21 and p28 (Figs. 3.3C-D), suggesting that type 2 cytokines contribute to the temperature-independent component of postnatal beiging.

We next analyzed UCP1 expression in iWAT from adult KO mice housed at 4^{o}C for 2 days and observed similar results to the postnatal time point, i.e. beiging in IL4/13-DKO was impaired, but not in IL4Ra-KO (Figs. 3.3E-F). In addition, no defect was observed in IL4Ra-KO on BL/6J background compared to BL/6J WT tissues (Fig. 3.3G). This was especially perplexing given that previous studies (Qiu et al. 2014) had reported defects in both cold-induced UCP1 expression and thermogenic function in IL4Ra-KO (BALB/cJ) mice. Nonetheless, our data showed that type 2 signaling is necessary for cold-induced beiging in adults, though the exact mechanism remains unclear. Given that all these immune mouse models are constitutive KO's, we attempted to parse the contribution of IL-4 at different time points with a rescue experiment. Briefly, IL4/13-DKO mice were treated with either saline or IL-4 complexed with anti-IL4 antibody (Odegaard et al. 2016) from p17-p31, housed at RT until 8 wks old, and then moved to 4^{o}C for 2 days. No difference was observed between IL4c- and saline-treated groups (Fig. 3.3H), which implied that type 2 signaling in the postnatal period alone was insufficient to license the adipocytes for future reactivation.

Finally, colonization by gut commensals modulates immune system development in postnatal mice (Gensollen et al. 2016; El Aidy et al. 2013) and plays a role in the adult cold-response (Chevalier et al. 2015; Ziętak et al. 2016), thus we asked whether absence of the microbiome had any effect on beiging. We analyzed iWAT from 4- and 9-wk-old Specific-Pathogen-Free (SPF) and Germ-Free (GF) mice housed at RT and observed no differences

between the groups (Fig. 3.3I). This suggests that microbiome colonization is not required for postnatal beiging, nor does it cause aberrant activation at RT in adults.

DISCUSSION

In this chapter, our goal was to identify temperature-independent drivers of beige fat recruitment; to that end, we established distinct roles for BCL6 and type 2 cytokine signaling in this process. Firstly, early deletion of BCL6 specifically in adipocyte precursors completely abrogated beiging in both postnatal and adult iWAT, confirming that it is required for beiging in a cell-intrinsic manner. Furthermore, later deletion with AdipoQ- and Ucp1-cre resulted in much less severe defects, strongly suggesting that BCL6 is primarily required for *de novo* beige differentiation. This was an unexpected result because BCL6 maintains BAT dormancy when that tissue is inactive under warm housing conditions (Kutyavin and Chawla 2019); thus we had hypothesized that it might perform a similar function in dormant ex-beige adipocytes. Having said that, brown and beige fat are ultimately derived from distinct progenitor lineages (M. Harms and Seale 2013; M. J. Harms et al. 2014); and thus ought to differ in some regulatory aspects.

Secondly, mice with global KO of the type 2 cytokines IL-4 and IL-13 exhibited significantly impaired beiging at both postnatal and adult time points. In addition, the postnatal defect was exacerbated when these mice were housed at thermoneutrality, which suggested that these cytokines are required for the temperature-independent component of beiging. Unfortunately, we lacked the genetic tools to distinguish between contributions at each time point; this matters in the context of constitutive deletions, as any phenotype observed at the adult time point could potentially be due solely to a prior developmental defect. In addition, we did not see any phenotype with mice lacking IL-4R or its downstream mediator STAT6 on both BL/6 and BALB/c backgrounds. One improbably explanation for these conflicting results could

be the presence of an as-yet-unknown non-canonical pathway, but a more likely one is that the observed phenotype in IL4/13-DKO is due to polymorphism of linked gene(s) near the IL-4/IL-13 genomic locus. These may have been carried over despite multiple generations of backcrossing, resulting in a phenotype that is unique to this KO line and absent in the IL4Ra-KO and STAT6-KO lines which were independently derived. Following up on these possibilities is beyond the scope of this work. In conclusion, we have identified cell-intrinsic (BCL6) and tissue-intrinsic (type 2 cytokines) signals that drive beiging in postnatal and adult iWAT.

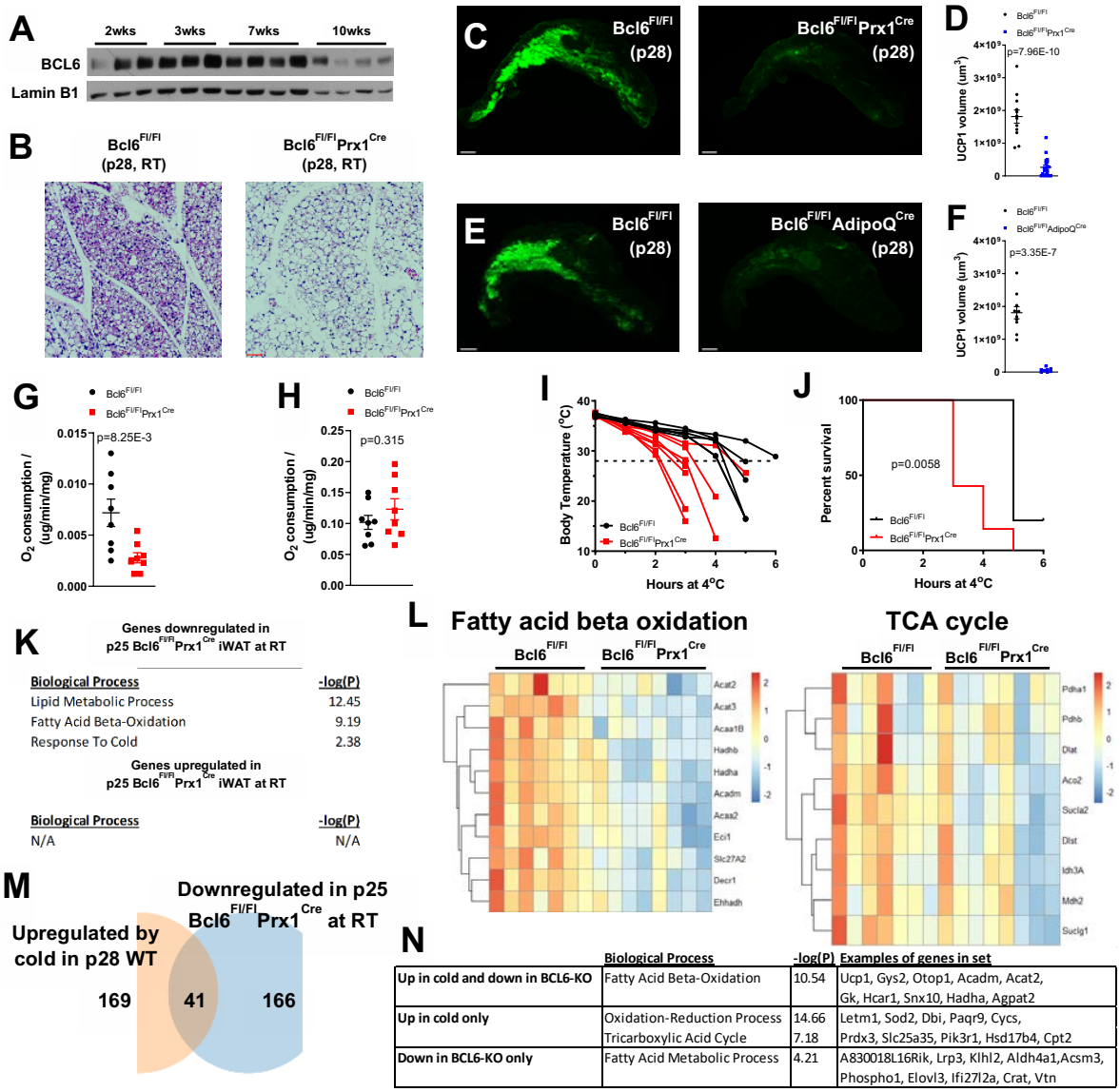

Figure 3.1: Adipocyte BCL6 is required for postnatal beiging but regulates distinct transcriptional pathways from cold-induced beige.

(A) Western blot for BCL6 in iWAT from male mice housed at RT. (B) Representative H&E stain of iWAT from p28 Bcl6$^{Fl/Fl}$Prx1^{Cre} mice housed at RT (scale bar = 50 μm). (C) Representative whole tissue UCP1 staining of iWAT from p28 Bcl6$^{Fl/Fl}$Prx1^{Cre} mice housed at RT (scale bar = 1 mm). (D) Quantification of UCP1 staining in (C). (E) UCP1 staining of iWAT from p28 Bcl6$^{Fl/Fl}$AdipoQ^{Cre} mice housed at RT (scale bar = 1 mm). (F) Quantification of UCP1 staining in (E). (G) Oxygen consumption rate of iWAT from p28 Bcl6$^{Fl/Fl}$Prx1^{Cre} mice housed at RT. (H) Oxygen consumption rate of BAT from p28 Bcl6$^{Fl/Fl}$Prx1^{Cre} mice housed at RT. (I) Rectal temperature of p28 Bcl6$^{Fl/Fl}$Prx1^{Cre} mice cold-challenged at 4°C. (J) Survival curve of p28 Bcl6$^{Fl/Fl}$Prx1^{Cre} mice cold-challenged at 4°C for up to 6 hrs. (K) GO analysis of pathways downregulated in iWAT from p25 Bcl6$^{Fl/Fl}$Prx1^{Cre} mice housed at RT (RNA-seq; n=7-8 per group). (L) Expression of metabolic genes downregulated in (K). (M) Comparison of cold-induced and BCL6-dependent genes from iWAT in young mice. (M) GO analysis of enriched pathways (FDR ≤ 0.05) and top 10 genes (fold change ≥1.5 and p-adj ≤0.05) per set in (N).

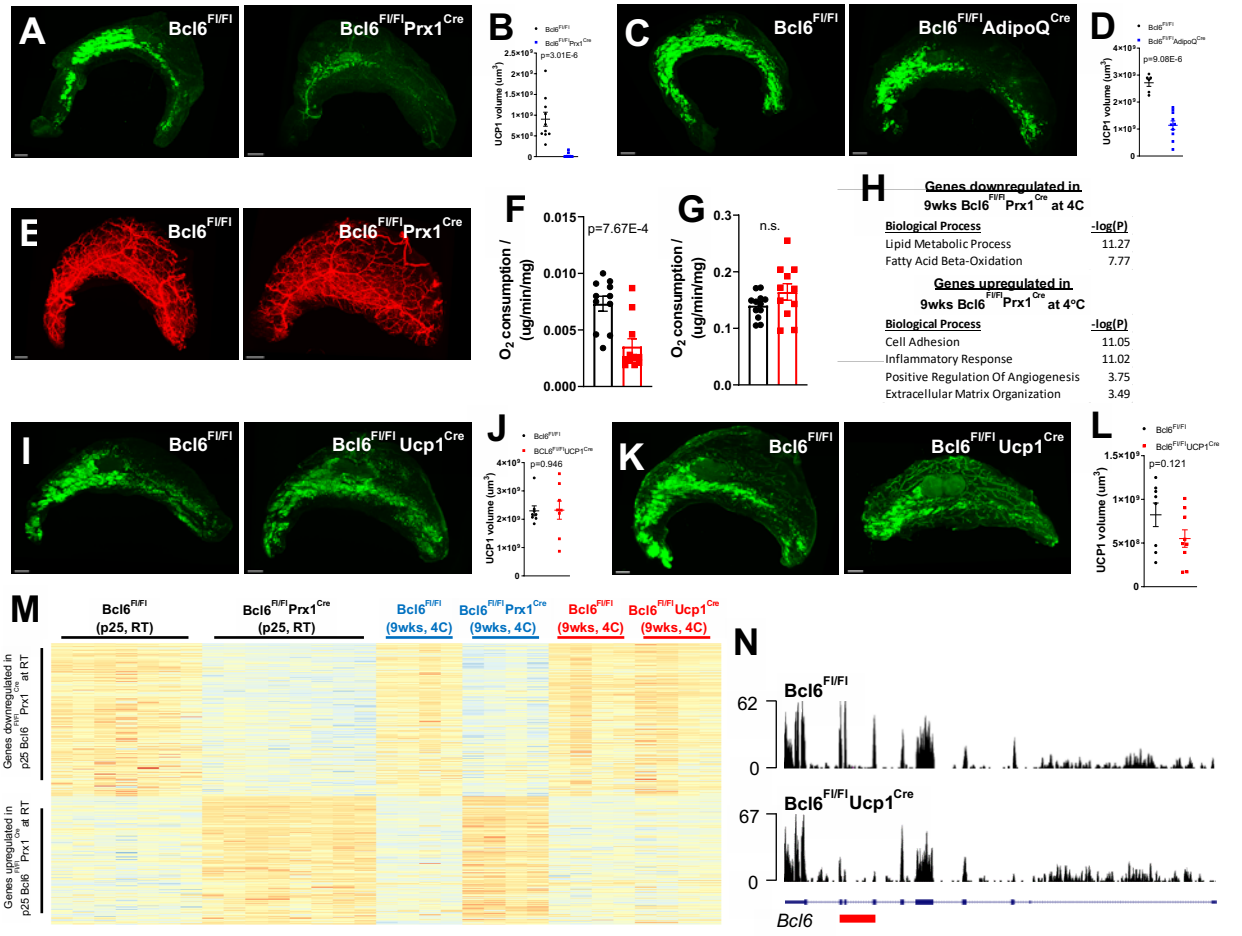

Figure 3.2: BCL6 is required for cold-induced beiging in adults, but not reactivation of dormant adipocytes.

(A) Representative whole tissue UCP1 staining of iWAT from 14 wk old Bcl6$^{Fl/Fl}$Prx1^{Cre} mice housed at 4°C for 2 days (scale bar = 1 mm). (B) Quantification of UCP1 staining in (A). (C) UCP1 staining of iWAT from 10 wk old Bcl6$^{Fl/Fl}$AdipoQ^{Cre} mice housed at 4°C for 2 days (scale bar = 1 mm). (D) Quantification of UCP1 volume in (C). (E) TH staining of iWAT from 8 wk old Bcl6$^{Fl/Fl}$Prx1^{Cre} mice housed at RT (scale bar = 1 mm). (F) Oxygen consumption of iWAT from 9-10 wk old Bcl6$^{Fl/Fl}$Prx1^{Cre} mice housed at 4°C for 2 days. (G) Same as (F) but for BAT. (H) GO analysis of pathways that were differentially expressed in iWAT from 9 wk old Bcl6$^{Fl/Fl}$Prx1^{Cre} mice housed at 4°C for 2 days. (I) UCP1 staining of iWAT from p28 Bcl6$^{Fl/Fl}$Ucp1^{Cre} mice housed at RT (scale bar = 1 mm). (J) Quantification of UCP1 staining in (G). (K) UCP1 staining of iWAT from 9 wk old Bcl6$^{Fl/Fl}$Ucp1^{Cre} mice housed at 4°C for 2 days (scale bar = 1 mm). (L) Quantification of UCP1 staining in (I). (M) Expression of young-BCL6-dependent genes in iWAT from p25 Bcl6$^{Fl/Fl}$Prx1^{Cre} RT, 9 wk old Bcl6$^{Fl/Fl}$Prx1^{Cre} 4°C, and 9wk old Bcl6$^{Fl/Fl}$Ucp1^{Cre} 4°C mice (RNA-seq; n=4-8 per group). (N) Genome browser tracks at *Bcl6* locus showing partial excision of exons 7-9 (red bar) in iWAT from 9 wk old Bcl6$^{Fl/Fl}$Ucp1^{Cre} mice housed at 4°C for 2 days.

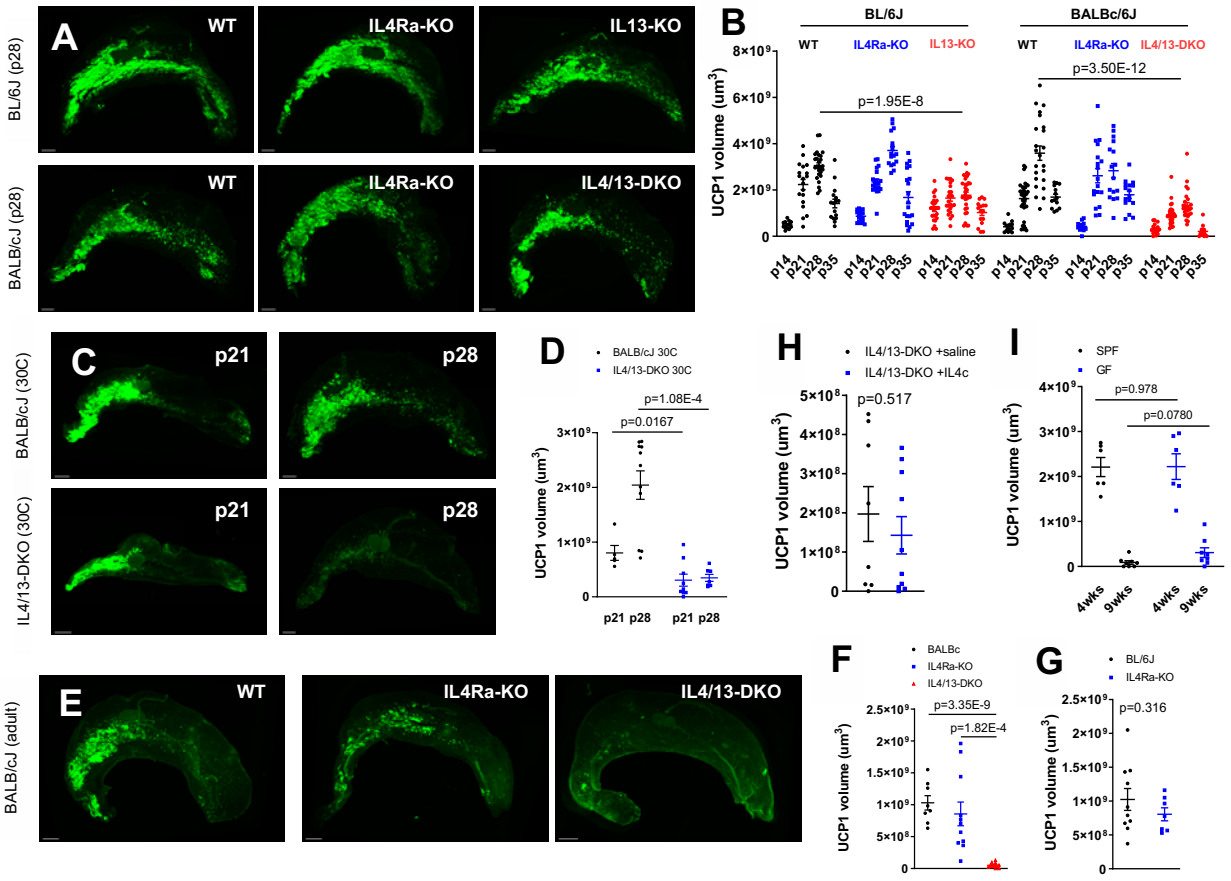

Figure 3.3: Immune signals play complicated roles in postnatal and adult beiging.

(A) Representative whole tissue UCP1 staining of iWAT from various p28 immune-KO mice housed at RT (scale bar = 1 mm). (B) Quantification of UCP1 staining in (A). (C) UCP1 staining of iWAT from young BALB/cJ and IL4/13-DKO mice born and housed at 30C (scale bar = 1 mm). (D) Quantification of UCP1 staining in (C). (E) UCP1 staining of iWAT from 12-15 wk old BALB/cJ, IL4Ra-KO, and IL4/13-DKO mice housed at 4°C for 2 days (scale bar = 1 mm). (F) Quantification of UCP1 staining in (E). (G) Quantification of UCP1 staining in iWAT from 12 wk old BL/6J and IL4Ra-KO mice housed at 4°C for 2 days. (H) Quantification of UCP1 staining in iWAT from 8 wk old IL4/13-DKO mice housed at 4°C for 2 days following treatment with IL4c (or saline) during the postnatal period. (I) Quantification of UCP1 staining of iWAT from 4 and 9 wk old Specific-Pathogen-Free (SPF) and Germ-Free (GF) BL/6J mice housed at RT.

METHODS

EXPERIMENTAL MODEL AND SUBJECT DETAILS

Mice

All animal studies were conducted under an approved Institutional Animal Care and Use Committee (IACUC) protocol at University of California, San Francisco (UCSF). All mice were congenic to the C57BL6/J background and housed in the mouse vivarium at ambient temperatures ranging between 4°C or 30°C as indicated. A 12-hour light:dark cycle was used, and food and water were available *ad libitum*. For room temperature (RT) housing, mouse cages were placed on racks exposed to the room atmosphere (~22°C). For housing at other temperatures, cages were placed in temperature-controlled chambers (Darwin Chambers or Power Scientific) set to the desired value. Unless otherwise indicated, mice were housed at a constant temperature from birth.

Cold tolerance tests were performed as previously described (Lee et al., 2015). Briefly, two mice were housed in each pre-chilled cage with food and water available *ad libitum*. Rectal temperature was measured hourly using a BAT-12 microprobe thermometer with RET-3 thermocouple (PhysiTemp). Per IACUC guidelines, survival was defined as a core temperature > 28°C. Similar housing conditions were used for 48-hour cold exposure studies.

Mice were fed normal chow diet (5053, Pico labs). Both male and female mice were used for all experiments (see figures for exact ages). C57BL/6J, *Bcl6*$^{Fl/Fl}$, *Prx1*^{Cre}, *AdipoQ*^{Cre}, *Ucp1*^{Cre}, BALB/cJ, *IL13-KO, IL4/13-DKO, and IL4Ra-KO* mice were purchased from Jackson Laboratories and bred in our vivarium. Germ-Free mice and Specific-Pathogen-Free controls were purchased from the UCSF Gnotobiotic Core. For all *in vivo* studies, cohorts of at least three mice per genotype or treatment group were used, and experiments were repeated two or three times independently.

Methods Details:

Tissue Clearing:

Inguinal white adipose tissue (iWAT) samples were processed using the recently published Adipo-Clear protocol (Chi et al., 2018). Briefly, samples were fixed overnight in 4% PFA, washed in PBS, and dehydrated via methanol gradient. They were then delipidated using dichloromethane (DCM), bleached in a hydrogen peroxide-DMSO solution overnight, and rehydrated via methanol gradient. Samples were incubated with primary followed by secondary antibodies (37^{o}C for 3 days each), with wash steps after each stain (see STAR Methods for full list of antibodies). Finally, they were dehydrated via methanol series, delipidated with DCM, then cleared in dibenzyl ether (DBE). All steps apart from antibody staining were carried out at RT with shaking.

3D Imaging:

Cleared samples were imaged on a Nikon AZ100 microscope that had been modified for light sheet imaging (UCSF Nikon Imaging Center), in conjunction with Micro-Manager software (https://micro-manager.org). Acquisition settings for whole-tissue and high-magnification zoomed shots were 1x objective / 10um step-size and 5x objective / 3um step-size respectively.

Image Processing and Quantification:

All 3D images were processed using Imaris x64 software (version 9.3.1, Bitplane), 2D snapshots taken using the snapshot function. For UCP1 volume quantification, the Surface tool was used to generate a mask of the UCP1-positive region, followed by automated calculation of the volume by the software.

Histology:

Freshly isolated iWAT was fixed in 10% formalin, and then submitted for embedding, sectioning,

and H&E staining at the UCSF Liver Center Pathology and Imaging Core in partnership with the Peninsular Histopathology Laboratory. H&E slides were scanned using an Axio Scan.Z1 (Zeiss).

RNA Isolation:

Snap-frozen iWAT samples were homogenized in Trisure (Bioline) using a TissueLyser II (Qiagen) for 2 minutes at 30 Hz. Phase separation was induced with 1-Bromo-3-chloropropane, followed by precipitation in isopropanol and two 70% ethanol washes. RNA concentration was measured with a Nanodrop 2000 spectrophotometer (Thermo Fisher Scientific).

Sequencing Library Preparation:

RNA-Seq libraries were constructed as described previously (Kutyavin and Chawla 2019). Briefly, the TruSeq Stranded mRNA Library Prep Kit (Illumina) was used according to the manufacturer's instructions with 2 µg of total RNA was used as the starting material. PolyA-containing RNA was purified and fragmented, followed by first and second strand cDNA synthesis, adapter ligation, and PCR amplification (15 cycles). A library size of 200-300 bp was verified by agarose gel electrophoresis and library concentration was measured with a Qubit dsDNA High Sensitivity Assay Kit and a Qubit 2.0 fluorimeter (Thermo Fisher Scientific).

Next Generation Sequencing:

Pooled library samples were diluted to 10 nM concentration and submitted to the UCSF CAT Core for sequencing on a HiSeq 4000 (single-read mode).

RNA-seq Analysis:

Analysis was performed as described previously (Kutyavin and Chawla 2019). Briefly, raw sequence data were pseudo-aligned to the mouse transcriptome (mm10, UCSC annotation) using Kallisto. Differential expression was defined as a fold change ≥1.5 and an adjusted p-value ≤0.05 and calculated using DESeq2. Heat maps were generated in R. Venn Diagrams were generated using BioVenn (https://www.biovenn.nl) and Venn Diagram Generator

(https://academo.org/demos/venn-diagram-generator/). Gene ontology enrichment analysis was performed using DAVID Bioinformatics Resources 6.8.

Tissue Oxygen Consumption:

Oxygen consumption measurement was performed as described previously (Kutyavin and Chawla 2019). Briefly, freshly isolated iWAT and BAT were finely minced, and the fragments resuspended in respiration buffer (PBS containing 20 mg/ml BSA, 25 mM glucose, and 1 mM pyruvate). The rate of oxygen consumption was recorded with a Mitocell S200 respirometry system (Strathkelvin Instruments). Data were analyzed with Strathkelvin 782 Oxygen System software (version 4.1).

Immunoblotting:

Western blotting for UCP1 and BCL6 was performed as described previously (Kutyavin and Chawla 2019). To prepare whole cell extracts, frozen tissue samples were placed into 2 mL tubes containing 0.5 mL of modified RIPA buffer (50 mM Tris-Cl, pH 7.5, 150 mM NaCl, 1% Nonidet P-40 substitute (Fluka), 0.1% SDS, 0.5% sodium deoxycholate, 1 mM EDTA, with 1:200 protease inhibitor cocktail (Sigma-Aldrich #P8340) and a metal bead, and homogenized in a TissueLyser II (Qiagen) for 120 seconds at 30 Hz. Nuclear extracts were prepared using NE-PER Nuclear and Cytoplasmic Extraction Reagents (Thermo Fisher Scientific #78833) according to the manufacturer's instructions. Protein concentration was measured with a Pierce BCA Protein Assay Kit (Thermo Fisher Scientific #23225) according to the manufacturer's instructions. Protein (5-30 µg) was diluted in sample buffer (62.5 mM Tris-Cl, pH 6.8, 10% glycerol, 2% SDS, 5% 2-mercaptoethanol, 0.008% bromophenol blue), incubated at 90° C for 5 minutes, separated by SDS–PAGE, and transferred to a 0.45 µm nitrocellulose membrane (Bio-Rad #1620115). The membrane was blocked with 5% nonfat dry milk in PBS containing 0.1% Tween-20 for 30 mins and probed with the primary and HRP-conjugated secondary antibodies diluted in PBS containing 0.1% Tween-20 and 2% BSA (see STAR Methods for full list of

antibodies). HSP90a/b and Lamin B1 were used as loading controls for whole cell extracts and nuclear extracts, respectively. Immunoblotted proteins were detected on HyBlot CL autoradiography film (Denville Scientific #1159M39) using ProSignal Pico chemiluminescent substrate (Prometheus Protein Biology Products #20-300) and Mini-Medical 90 X-ray Film 27 Processor (AFP Imaging #9992305300).

Chapter 4 :

Concluding Remarks and Future Directions

What is a legacy? It's planting seeds in a garden you never get to see.

—Lin-Manuel Miranda, *Hamilton: An American Musical*

The work presented here shows that beige fat recruitment in inguinal white adipose tissue (iWAT) follows a consistent spatial pattern in both postnatal and adult time points, and that despite this superficial similarity, different regulatory pathways predominate at each stage of life. Postnatal beiging is absolutely dependent on B-cell lymphoma 6 (BCL6) but not adrenergic signaling, whereas adult beiging is only partially dependent on the former and requires the latter. Furthermore, environmental cold induced distinct transcriptional profiles in postnatal versus adult iWAT, underscoring how the tissue is fundamentally different at these two time points despite performing a similar thermogenic function in both.

Why is postnatal beige fat so different from its future self? It may have evolved because neonates are intrinsically vulnerable to heat loss compared to adults, due to having reduced insulation from fur and subcutaneous fat coupled with a higher surface-area-to-volume ratio (Nedergaard and Cannon 2014). In addition, they have limited behavioral options to mitigate environmental cold apart from huddling with their parents and littermates (Smith and Horwitz 1969; Chabowska-Kita and Kozak 2016). Hence the need for a constitutive minimum level of thermogenic potential regardless of environmental conditions to supplement brown adipose tissue (BAT) function. Furthermore, weaning (~p21 in mice) is a significant transition for young animals as they enter a new independent phase of life and may be associated with added environmental cold stress, as evinced by a transient increase in BAT UCP1 expression at that time point (Odegaard et al. 2016).

Although the sympathetic nervous system (SNS) was not required for transcription of UCP1 or associated metabolic pathways (e.g. beta oxidation), ablation of SNS nerves did specifically result in downregulation of cholesterol / steroid synthesis pathways. These pathways have been implicated in both lipid (Yeh et al. 2018) and glucose (Okin and Medzhitov 2016) metabolism, which suggests that the SNS may influence thermogenic function indirectly by modulating the availability of fuel sources in adipocytes. In addition, our pilot experiments

revealed a potential defect in cold-tolerance in both postnatal and adult TrkA-KO mice (data not shown), suggesting that the nerves might be required to 'switch on' the thermogenic machinery after it has been properly expressed. Nonetheless, we were unable to parse the role of beige fat versus BAT due to the systemic nature of the Th^{Cre} deletion. Ultimately, iWAT from adult TrkA-KO mice responded normally to adrenergic agonist (CL-316,243) treatment, which implied that SNS nerves are not required to license thermogenic function during development. One intriguing question is why thermoneutral housing reduces the amplitude of postnatal beiging, but SNS deficiency does not. This result implies that the temperature-sensitive component of beiging is not mediated by the SNS, and it would be interesting if future studies were to identify this unknown actor.

We also identified a critical role for BCL6 in postnatal beige recruitment, though it was not required in adults for either reactivation of ex-beige adipocytes (Ucp1-KO mice), or transdifferentiation of mature white adipocytes (AdipoQ-KO mice). Therefore, by process of elimination, its influence at the adult time point is restricted to the *de novo* differentiation of adipocyte precursors. That BCL6 was not required for reactivation was unexpected given that BCL6 is required to maintain BAT dormancy under warm housing conditions (Kutyavin and Chawla 2019). One possible explanation for this discrepancy is that dormant BAT consists of brown adipocytes with thermogenic character (e.g. UCP1 expression), whereas dormant iWAT consists almost exclusively of UCP1-negative white adipocytes, i.e. BCL6 maintains thermogenic identity (brown and beige adipocytes) but not potential (ex-beige white adipocytes). This is supported by the transcriptional data showing that in addition to UCP1 expression, BCL6 also drives expression of fatty acid beta oxidation genes in iWAT of both postnatal and adult mice (our data), as well as in adult BAT (Kutyavin and Chawla 2019).

Finally, we found that type 2 cytokine signaling (IL-4 and to a lesser extent, IL-13) were involved in both postnatal and adult cold-induced beige recruitment. Furthermore, postnatal

IL4/13-DKO mice housed at thermoneutrality exhibited an even more severe beiging defect than at room temperature, suggesting that cytokine signaling is involved in the temperature-independent part of this process. As for the phenotype in adults, this had been shown previously (Qiu et al. 2014; M.-W. Lee et al. 2014), though there was some conflicting data which suggested the existence of an unknown non-canonical signaling route for these cytokines that bypasses the IL4-receptor. This could explain why a beiging defect was observed in cytokine- but not receptor-knockout mice. On a separate note, BCL6 and IL-4 are both heavily involved in the lineage commitment of T follicular helper (T_{FH}) and germinal center (GC) B cells (Johnston et al. 2009; Bélanger and Crotty 2016). This raises the tantalizing possibility that a parallel interaction may exist in adipocytes since both signals are involved in *de novo* beige differentiation (M.-W. Lee et al. 2014); this hypothesis may warrant further investigation.

Prior studies have either described postnatal beige fat kinetics in passing (Gouon-Evans and Pollard 2002; Master et al. 2002; Odegaard et al. 2016), or focused on specific aspects such as the temperature-dependence of postnatal beiging (Chabowska-Kita et al. 2015) and the signaling requirements for beige adipocyte dormancy (Y. Wang et al. 2017). To our knowledge this dissertation is the first attempt at an in-depth, multi-dimensional characterization of the spatiotemporal and regulatory aspects of postnatal versus adult beige fat recruitment. We propose that postnatal beiging has long-term implications for cold-induced recruitment in later life, and that there is much to be learned in this relatively uncharted space in beige fat biology.

References

Aidy, Sahar El, Guido Hooiveld, Valentina Tremaroli, Fredrik Bäckhed, and Michiel Kleerebezem. 2013. “The Gut Microbiota and Mucosal Homeostasis: Colonized at Birth or at Adulthood, Does It Matter?” *Gut Microbes* 4 (2): 118–24.

Balaz, Miroslav, Anton S Becker, Lucia Balazova, Leon Straub, Julian Müller, Gani Gashi, Claudia Irene Maushart, et al. 2019. “Inhibition of Mevalonate Pathway Prevents Adipocyte Browning in Mice and Men by Affecting Protein Prenylation.” *Cell Metabolism* 29 (4): 901-916.e8. https://doi.org/10.1016/j.cmet.2018.11.017.

Bélanger, Simon, and Shane Crotty. 2016. “Dances with Cytokines, Featuring TFH Cells, IL-21, IL-4 and B Cells.” *Nature Immunology* 17 (10): 1135–36. https://doi.org/10.1038/ni.3561.

Berry, Ryan, and Matthew S Rodeheffer. 2013. “Characterization of the Adipocyte Cellular Lineage in Vivo.” *Nature Cell Biology* 15 (3): 302–8. https://doi.org/10.1038/ncb2696.

Borden, Philip, Jessica Houtz, Steven D. Leach, and Rejji Kuruvilla. 2013. “Sympathetic Innervation during Development Is Necessary for Pancreatic Islet Architecture and Functional Maturation.” *Cell Reports* 4 (2): 287–301. https://doi.org/10.1016/j.celrep.2013.06.019.

Brestoff, Jonathan R., Brian S. Kim, Steven a. Saenz, Rachel R. Stine, Laurel a. Monticelli, Gregory F. Sonnenberg, Joseph J. Thome, et al. 2014. “Group 2 Innate Lymphoid Cells Promote Beiging of White Adipose Tissue and Limit Obesity.” *Nature*, December. https://doi.org/10.1038/nature14115.

Cannon, Barbara, and Jan Nedergaard. 2004. “Brown Adipose Tissue: Function and Physiological Significance.” *Physiological Reviews* 84 (1): 277–359. https://doi.org/10.1152/physrev.00015.2003.

———. 2011. “Nonshivering Thermogenesis and Its Adequate Measurement in Metabolic Studies.” *Journal of Experimental Biology* 214 (2): 242–53. https://doi.org/10.1242/jeb.050989.

Chabowska-Kita, Agnieszka, and Leslie P. Kozak. 2016. “The Critical Period for Brown Adipocyte Development: Genetic and Environmental Influences.” *Obesity* 24 (2): 283–90. https://doi.org/10.1002/oby.21376.

Chabowska-Kita, Agnieszka, Anna Trabczynska, Agnieszka Korytko, Monika M. Kaczmarek, and Leslie P. Kozak. 2015. “Low Ambient Temperature during Early Postnatal Development Fails to Cause a Permanent Induction of Brown Adipocytes.” *FASEB Journal* 29 (8): 3238–52. https://doi.org/10.1096/fj.15-271395.

Chen, Xi, Haihong Ye, Rejji Kuruvilla, Narendrakumar Ramanan, Katherine W Scangos, Chao Zhang, Nicolas M Johnson, Pamela M England, Kevan M Shokat, and David D Ginty. 2005. “A Chemical-Genetic Approach to Studying Neurotrophin Signaling.” *Neuron* 46 (1): 13–21. https://doi.org/10.1016/j.neuron.2005.03.009.

Chen, Yong, Kenji Ikeda, Takeshi Yoneshiro, Annarita Scaramozza, Kazuki Tajima, Qiang Wang, Kyeongkyu Kim, et al. 2019. “Thermal Stress Induces Glycolytic Beige Fat Formation via a Myogenic State.” *Nature* 565 (7738): 180–85. https://doi.org/10.1038/s41586-018-0801-z.

Chevalier, Claire, Ozren Stojanović, Didier J. Colin, Nicolas Suarez-Zamorano, Valentina Tarallo, Christelle Veyrat-Durebex, Dorothée Rigo, et al. 2015. “Gut Microbiota Orchestrates Energy Homeostasis during Cold.” *Cell* 163 (6): 1360–74. https://doi.org/10.1016/j.cell.2015.11.004.

Chi, Jingyi, Zhuhao Wu, Chan Hee J. Choi, Lily Nguyen, Saba Tegegne, Sarah E. Ackerman, Audrey Crane, François Marchildon, Marc Tessier-Lavigne, and Paul Cohen. 2018. “Three-

Dimensional Adipose Tissue Imaging Reveals Regional Variation in Beige Fat Biogenesis and PRDM16-Dependent Sympathetic Neurite Density." *Cell Metabolism* 27 (1): 226-236.e3. https://doi.org/10.1016/j.cmet.2017.12.011.

Contreras, G. Andres, Yun Hee Lee, Emilio P. Mottillo, and James G. Granneman. 2014. "Inducible Brown Adipocytes in Subcutaneous Inguinal White Fat: The Role of Continuous Sympathetic Stimulation." *American Journal of Physiology - Endocrinology and Metabolism* 307 (9): E793–99. https://doi.org/10.1152/ajpendo.00033.2014.

Gensollen, Thomas, Shankar S Iyer, Dennis L Kasper, and Richard S Blumberg. 2016. "How Colonization by Microbiota in Early Life Shapes the Immune System." *Science* 352 (6285): 539–44.

Gouon-Evans, Valérie, and Jeffrey W. Pollard. 2002. "Unexpected Deposition of Brown Fat in Mammary Gland during Postnatal Development." *Molecular Endocrinology* 16 (11): 2618–27. https://doi.org/10.1210/me.2001-0337.

Gulyaeva, Olga, Jon Dempersmier, and Hei Sook Sul. 2019. "Genetic and Epigenetic Control of Adipose Development ☆." *BBA - Molecular and Cell Biology of Lipids* 1864 (1): 3–12. https://doi.org/10.1016/j.bbalip.2018.04.016.

Harms, Matthew J, Jeff Ishibashi, Wenshan Wang, Hee-Woong Lim, Susumu Goyama, Tomohiko Sato, Mineo Kurokawa, Kyoung-Jae Won, and Patrick Seale. 2014. "Prdm16 Is Required for the Maintenance of Brown Adipocyte Identity and Function in Adult Mice." *Cell Metabolism* 19 (4): 593–604. https://doi.org/10.1016/j.cmet.2014.03.007.

Harms, Matthew, and Patrick Seale. 2013. "Brown and Beige Fat: Development, Function and Therapeutic Potential." *Nature Medicine* 19 (10): 1252–63. https://doi.org/10.1038/nm.3361.

Hollister, Kristin, Saritha Kusam, Hao Wu, Ninah Clegg, Arpita Mondal, Deepali V Sawant, and Alexander L Dent. 2013. “Insights into the Role of Bcl6 in Follicular Th Cells Using a New Conditional Mutant Mouse Model.” *Journal of Immunology (Baltimore, Md. : 1950)* 191 (7): 3705–11. https://doi.org/10.4049/jimmunol.1300378.

Hong, Ki Yong, Hosung Bae, Intae Park, Dae Young Park, Kyun Hoo Kim, Yoshiaki Kubota, Eui Sic Cho, et al. 2015. “Perilipin^{+} Embryonic Preadipocytes Actively Proliferate along Growing Vasculatures for Adipose Expansion.” *Development (Cambridge)* 142 (15): 2623–32. https://doi.org/10.1242/dev.125336.

Jiang, Haochen, Xiaofan Ding, Haochen Jiang, Xiaofan Ding, Ying Cao, Huanhuan Wang, and Wenwen Zeng. 2017. “Short Article Dense Intra-Adipose Sympathetic Arborizations Are Essential for Cold-Induced Beiging of Mouse White Short Article Dense Intra-Adipose Sympathetic Arborizations Are Essential for Cold-Induced Beiging of Mouse White Adipose Tissue.” *Cell Metabolism*, 1–7. https://doi.org/10.1016/j.cmet.2017.08.016.

Johnston, Robert J., Amanda C. Poholek, Daniel DiToro, Isharat Yusuf, Danelle Eto, Burton Barnett, Alexander L. Dent, Joe Craft, and Shane Crotty. 2009. “Bcl6 and Blimp-1 Are Reciprocal and Antagonistic Regulators of T Follicular Helper Cell Differentiation.” *Science* 325 (5943): 1006–10. https://doi.org/10.1126/science.1175870.

Kaji, Tomohiro, Akiko Ishige, Masaki Hikida, Junko Taka, Atsushi Hijikata, Masato Kubo, Takeshi Nagashima, et al. 2012. “Distinct Cellular Pathways Select Germline-Encoded and Somatically Mutated Antibodies into Immunological Memory.” *The Journal of Experimental Medicine* 209 (11): 2079–97. https://doi.org/10.1084/jem.20120127.

Kutyavin, Vassily I., and Ajay Chawla. 2019. “BCL6 Regulates Brown Adipocyte Dormancy to Maintain Thermogenic Reserve and Fitness.” *Proceedings of the National Academy of Sciences*, 201907308. https://doi.org/10.1073/pnas.1907308116.

Lasar, D., A. Julius, T. Fromme, and M. Klingenspor. 2013. “Browning Attenuates Murine White Adipose Tissue Expansion during Postnatal Development.” *Biochimica et Biophysica Acta (BBA) - Molecular and Cell Biology of Lipids* 1831 (5): 960–68. https://doi.org/https://doi.org/10.1016/j.bbalip.2013.01.016.

Lee, Min-Woo, Justin I. Odegaard, Lata Mukundan, Yifu Qiu, Ari B. Molofsky, Jesse C. Nussbaum, Karen Yun, Richard M. Locksley, and Ajay Chawla. 2014. “Activated Type 2 Innate Lymphoid Cells Regulate Beige Fat Biogenesis.” *Cell*, December, 1–14. https://doi.org/10.1016/j.cell.2014.12.011.

Lee, Yun-hee, Anelia P Petkova, and James G Granneman. 2013. “Identification of an Adipogenic Niche for Adipose Tissue Remodeling and Restoration.” *Cell Metabolism* 18 (3): 355–67. https://doi.org/10.1016/j.cmet.2013.08.003.

Lee, Yun-hee, Anelia P Petkova, Anish A Konkar, and James G Granneman. 2019. “Cellular Origins of Cold-Induced Brown Adipocytes in Adult Mice.” https://doi.org/10.1096/fj.14-263038.

Lee, Yun-Hee, Anelia P Petkova, Emilio P Mottillo, and James G Granneman. 2012. “In Vivo Identification of Bipotential Adipocyte Progenitors Recruited by B3-Adrenoceptor Activation and High-Fat Feeding.” *Cell Metabolism* 15 (4): 480–91. https://doi.org/10.1016/j.cmet.2012.03.009.

Master, Stephen R., Jennifer L. Hartman, Celina M. D’Cruz, Susan E. Moody, Elizabeth A. Keiper, Seung I. Ha, James D. Cox, George K. Belka, and Lewis A. Chodosh. 2002. “Functional Microarray Analysis of Mammary Organogenesis Reveals a Developmental Role in Adaptive Thermogenesis.” *Molecular Endocrinology* 16 (6): 1185–1203. https://doi.org/10.1210/mend.16.6.0865.

McCormick, Sarah M., and Nicola M. Heller. 2015. “Commentary: IL-4 and IL-13 Receptors and

Signaling." *Cytokine* 75 (1): 38–50. https://doi.org/10.1016/j.cyto.2015.05.023.

Nedergaard, Jan, and Barbara Cannon. 2014. "The Browning of White Adipose Tissue: Some Burning Issues." *Cell Metabolism* 20 (3): 396–407. https://doi.org/10.1016/j.cmet.2014.07.005.

Nguyen, Khoa D, Yifu Qiu, Xiaojin Cui, Y P Sharon Goh, Julia Mwangi, Tovo David, Lata Mukundan, Frank Brombacher, Richard M Locksley, and Ajay Chawla. 2011. "Alternatively Activated Macrophages Produce Catecholamines to Sustain Adaptive Thermogenesis." *Nature* 480 (7375): 104–8. https://doi.org/10.1038/nature10653.

Nguyen, Ngoc Ly T, Jessica Randall, Bruce W Banfield, and Timothy J Bartness. 2014. "Central Sympathetic Innervations to Visceral and Subcutaneous White Adipose Tissue." *American Journal of Physiology. Regulatory, Integrative and Comparative Physiology*, January, 404–13. https://doi.org/10.1152/ajpregu.00552.2013.

Odegaard, Justin I., Min Woo Lee, Yoshitaka Sogawa, Ambre M. Bertholet, Richard M. Locksley, David E. Weinberg, Yuriy Kirichok, Rahul C. Deo, and Ajay Chawla. 2016. "Perinatal Licensing of Thermogenesis by IL-33 and ST2." *Cell* 166 (4): 841–54. https://doi.org/10.1016/j.cell.2016.06.040.

Okin, Daniel, and Ruslan Medzhitov. 2016. "The Effect of Sustained Inflammation on Hepatic Mevalonate Pathway Results in Hyperglycemia." *Cell* 165 (2): 343–56. https://doi.org/10.1016/j.cell.2016.02.023.

Qiu, Yifu, Khoa D. Nguyen, Justin I. Odegaard, Xiaojin Cui, Xiaoyu Tian, Richard M. Locksley, Richard D. Palmiter, and Ajay Chawla. 2014. "Eosinophils and Type 2 Cytokine Signaling in Macrophages Orchestrate Development of Functional Beige Fat." *Cell* 157 (6): 1292–1308. https://doi.org/10.1016/j.cell.2014.03.066.

Roh, Hyun Cheol, Linus T.Y. Tsai, Mengle Shao, Danielle Tenen, Yachen Shen, Manju Kumari, Anna Lyubetskaya, et al. 2018. “Warming Induces Significant Reprogramming of Beige, but Not Brown, Adipocyte Cellular Identity.” *Cell Metabolism* 27 (5): 1121-1137.e5. https://doi.org/10.1016/j.cmet.2018.03.005.

Rosenwald, Matthias, Aliki Perdikari, Thomas Rülicke, and Christian Wolfrum. 2013. “Bi-Directional Interconversion of Brite and White Adipocytes.” *Nature Cell Biology* 15 (6): 659–67. https://doi.org/10.1038/ncb2740.

Sanchez-Gurmaches, Joan, Wen Yu Hsiao, and David A. Guertin. 2015. “Highly Selective in Vivo Labeling of Subcutaneous White Adipocyte Precursors with Prx1-Cre.” *Stem Cell Reports* 4 (4): 541–50. https://doi.org/10.1016/j.stemcr.2015.02.008.

Senagolage, Madhavi D., Meredith A. Sommars, Krithika Ramachandran, Christopher R. Futtner, Yasuhiro Omura, Amanda L. Allred, Jianing Wang, et al. 2018. “Loss of Transcriptional Repression by BCL6 Confers Insulin Sensitivity in the Setting of Obesity.” *Cell Reports* 25 (12): 3283-3298.e6. https://doi.org/10.1016/j.celrep.2018.11.074.

Slavin, B G, and K W Ballard. 1978. “Morphological Studies on the Adrenergic Innervation of White Adipose Tissue.” *The Anatomical Record* 191 (3): 377–89. https://doi.org/10.1002/ar.1091910310.

Smith, Robert Emrie, and A Horwitz. 1969. “Brown Fat and Thermogenesis.” *Physiological Reviews* 49 (2): 330–425.

Spellberg, B, and J E Jr Edwards. 2001. “Type 1/Type 2 Immunity in Infectious Diseases.” *Clinical Infectious Diseases : An Official Publication of the Infectious Diseases Society of America* 32 (1): 76–102. https://doi.org/10.1086/317537.

Stearns, Stephen C. 1992. *The Evolution of Life Histories*.

Wang, Qiong A., Anying Song, Wanze Chen, Petra C. Schwalie, Fang Zhang, Lavanya Vishvanath, Lei Jiang, et al. 2018. “Reversible De-Differentiation of Mature White Adipocytes into Preadipocyte-like Precursors during Lactation.” *Cell Metabolism* 28 (2): 282-288.e3. https://doi.org/10.1016/j.cmet.2018.05.022.

Wang, Qiong A, Caroline Tao, Rana K Gupta, and Philipp E Scherer. 2013. “Tracking Adipogenesis during White Adipose Tissue Development, Expansion and Regeneration.” *Nature Medicine* 19 (10): 1338–44. https://doi.org/10.1038/nm.3324.

Wang, Yangmeng, Esther Paulo, Dongmei Wu, Yixuan Wu, Wendong Huang, Ajay Chawla, and Biao Wang. 2017. “Adipocyte Liver Kinase B1 Suppresses Beige Adipocyte Renaissance through Class IIa Histone Deacetylase 4.” *Diabetes* 66 (12): 2952–63. https://doi.org/10.2337/db17-0296.

Wu, Jun, Pontus Boström, Lauren M Sparks, Li Ye, Jang Hyun Choi, An-Hoa Giang, Melin Khandekar, et al. 2012. “Beige Adipocytes Are a Distinct Type of Thermogenic Fat Cell in Mouse and Human.” *Cell* 150 (2): 366–76. https://doi.org/10.1016/j.cell.2012.05.016.

Yeh, Yu-Sheng, Huei-Fen Jheng, Mari Iwase, Minji Kim, Shinsuke Mohri, Jungin Kwon, Satoko Kawarasaki, et al. 2018. “The Mevalonate Pathway Is Indispensable for Adipocyte Survival.” *IScience* 9 (November): 175–91. https://doi.org/10.1016/j.isci.2018.10.019.

Zeng, Wenwen, Roksana M. Pirzgalska, Mafalda M.A. Pereira, Nadiya Kubasova, Andreia Barateiro, Elsa Seixas, Yi-Hsueh Lu, et al. 2015. “Sympathetic Neuro-Adipose Connections Mediate Leptin-Driven Lipolysis.” *Cell* 163 (1): 84–94. https://doi.org/10.1016/j.cell.2015.08.055.

Zeng, Xing, Mengchen Ye, Jon M. Resch, Mark P. Jedrychowski, Bo Hu, Bradford B. Lowell, David D. Ginty, and Bruce M. Spiegelman. 2019. “Innervation of Thermogenic Adipose Tissue via a Calsyntenin 3β–S100b Axis.” *Nature* 569 (7755): 229–35.

https://doi.org/10.1038/s41586-019-1156-9.

Zhang, Wei, and Sheng Bi. 2015. “Hypothalamic Regulation of Brown Adipose Tissue Thermogenesis and Energy Homeostasis.” *Frontiers in Endocrinology* 6 (August): 136. https://doi.org/10.3389/fendo.2015.00136.

Ziętak, Marika, Petia Kovatcheva-Datchary, Lidia H Markiewicz, Marcus Ståhlman, Leslie P Kozak, and Fredrik Bäckhed. 2016. “Altered Microbiota Contributes to Reduced Diet-Induced Obesity upon Cold Exposure.” *Cell Metabolism* 23 (6): 1216–23. https://doi.org/https://doi.org/10.1016/j.cmet.2016.05.001.

Publishing Agreement

It is the policy of the University to encourage the distribution of all theses, dissertations, and manuscripts. Copies of all UCSF theses, dissertations, and manuscripts will be routed to the library via the Graduate Division. The library will make all theses, dissertations, and manuscripts accessible to the public and will preserve these to the best of their abilities, inperpetuity.

Author Signature

09.08.2019

Date